Horus—A Fully Digital Polarimetric Phased Array Radar for Next-Generation Weather Observations

Robert D. Palmer[ID], *Fellow, IEEE*, Mark B. Yeary[ID], *Fellow, IEEE*, David Schvartzman[ID], *Senior Member, IEEE*,
Jorge L. Salazar-Cerreno[ID], *Senior Member, IEEE*, Caleb Fulton[ID], *Senior Member, IEEE*,
Matthew McCord, *Member, IEEE*, Boonleng Cheong[ID], David Bodine[ID], *Member, IEEE*,
Pierre Kirstetter[ID], *Senior Member, IEEE*, Hjalti H. Sigmarsson[ID], *Senior Member, IEEE*,
Tian-You Yu[ID], *Member, IEEE*, Dušan Zrnić[ID], *Life Fellow, IEEE*, Redmond Kelley,
John Meier[ID], and Matthew Herndon[ID], *Member, IEEE*

Abstract— Weather radars have become indispensable to meteorologists and the general public for both understanding and awareness of high-impact weather events and as part of the operational warning infrastructure. In the U.S., the operational weather radar network is composed of approximately 160 WSR-88D radars, which are S-band, dish-based, polarimetric Doppler radars. This work reports on the development of a fully digital phased array weather radar that is being used to assess the potential of such technology as a replacement for the WSR-88D radars. The "Horus" radar is a truck-based, S-band, fully digital polarimetric phased array radar. Fully digital systems hold promise for meeting some of the greatest technical challenges facing the meteorological community, such as the effective integration of dual-polarization capability with phased array beam agility. This paper describes the fully digital Horus phased array weather radar that was recently completed by the Advanced Radar Research Center (ARRC) at the University of Oklahoma (OU). An overview of the advantages and challenges facing fully digital arrays for weather observations is provided along with potential mitigation strategies. Initial weather observations with Horus are given with the goal of assessing the radar scanning capabilities and most importantly the polarimetric quality. Finally, a vision for the future of next-generation weather radar operations is given with an eye toward leveraging the scalable design of Horus for high-resolution weather observations.

Index Terms— Phased arrays, weather radar, fully digital radar.

Robert D. Palmer, David Schvartzman, and David Bodine are with the Advanced Radar Research Center and the School of Meteorology, The University of Oklahoma, Norman, OK 73019 USA (e-mail: rpalmer@ou.edu).

Mark B. Yeary, Jorge L. Salazar-Cerreno, Caleb Fulton, Hjalti H. Sigmarsson, and Tian-You Yu are with the Advanced Radar Research Center and the School of Electrical and Computer Engineering, The University of Oklahoma, Norman, OK 73019 USA.

Matthew McCord, Boonleng Cheong, Redmond Kelley, John Meier, and Matthew Herndon are with the Advanced Radar Research Center, The University of Oklahoma, Norman, OK 73019 USA.

Pierre Kirstetter is with the Advanced Radar Research Center, the School of Meteorology, and the School of Civil Engineering and Environmental Science, The University of Oklahoma, Norman, OK 73019 USA.

Dušan Zrnić is with the NOAA National Severe Storms Laboratory, Norman, OK 73072 USA.

Digital Object Identifier 10.1109/TRS.2023.3280033

I. INTRODUCTION

WEATHER radar is the most important tool for observation and warning of increasingly frequent severe weather events. Extreme weather can disrupt communities, negatively impact commerce, civil operations, and cause billions of dollars in damage annually across the globe (e.g., [1]). Unfortunately, current operational weather dish-based radars were not designed to capture rapidly evolving processes that lead to extreme events. Significant improvements in the forecasting of high-impact weather require a new radar design that provides the needed spatial and temporal resolution along with the scanning capabilities afforded by phased array radar (PAR) technology [2], [3], [4], [5], [6], [7].

Polarimetric PAR is emerging as a promising technology for the next generation of weather radars due to its superior capabilities for capturing the microphysics and dynamics of a wide variety of rapidly evolving atmospheric phenomena across scales [2], [8], [9], [10]. Planar PAR antennas with electronic scanning only in elevation (mechanical in azimuth) avoid the issue of tilting the intended polarization axes, i.e., modulation on only one axis of the Poincaré sphere is needed. Such strategies have seen widespread implementation in Japan [11], [12], China [13], [14], and in the U.S. with the nascent Polarimetric Atmospheric Imaging Radar (PAIR) [15]. The Advanced Technology Demonstrator (ATD) [8] is a planar PAR capable of two-dimensional scanning, which requires polarimetric calibration per beamsteering position [16], [17]. A unique cylindrical polarimetric phased array radar (CPPAR) design has also been investigated [18], [19]. It is based on theoretical studies that showed the effectiveness of such designs for maintaining polarization orthogonality, which is needed for accurate polarimetric PAR observations.

The most advanced PAR architecture is a fully digital design, which holds promise for overcoming the challenge of combining polarimetric and PAR technologies [20], [21]. Via element-level control, robust mutual-coupling-based polarimetric "self" calibration is possible, thus having the highest likelihood of attaining accurate rapid-scanning polarimetric observations for long periods without the need for re-calibration. Further, fully digital technology is capable of emulating most other PAR architectures, as virtual

Fig. 1. Photograph of the fully digital S-band Horus phased array weather radar. The radome has been removed to reveal the 25 8 × 8 dual-polarization antenna panels (1,600 radiating elements). The corner panels have a slightly different color but are functionally identical.

subarrays can be defined by appropriately combining digital element-level signals. This feature makes an all-digital architecture useful for the assessment of competing radar designs.

With support from NOAA's National Severe Storms Laboratory (NSSL), the Advanced Radar Research Center (ARRC) at the University of Oklahoma (OU) has developed a fully digital polarimetric rotating PAR system called "Horus" [22], [23], the ancient Egyptian sky god with *the all-seeing eye*. A photograph of the Horus radar without its radome is shown in Fig. 1. Horus' fully digital architecture will enable rapid (volume scans in seconds) and adaptive scanning. By uniquely obtaining nearly continuous vertical sampling, Horus observations will more accurately capture 4D microphysical processes, including processes key to understanding and predicting the formation of severe hazards (e.g., tornadoes, hail, flooding). Pristine dual-polarization data, achieved by exploiting the all-digital architecture, will improve operational quantitative precipitation estimation as well as understanding of microphysical processes. Horus will operate with minimal attenuation and excellent sensitivity in the S band (2.7–3.1 GHz), which is ideal for atmospheric observations as scattering physics (at that band) are well-understood and the observational range is large. System integration of the Horus radar was recently completed at the ARRC, and initial deployments for polarimetric weather measurements are ongoing.

Here, we motivate the fully digital architecture of Horus for weather observations and give a system overview. Challenges of fully digital PARs and potential solutions are also provided, along with initial polarimetric weather measurements showing a glimpse of the potential of fully digital PARs for high-resolution weather observations.

II. MOTIVATION FOR WEATHER OBSERVATIONS

A. High Temporal Resolution and Spatial Sampling

Due to the scattering properties of hydrometeors, operational weather radars in the U.S. operate in the S-band [24], which minimizes attenuation and provides observations that typically hold to the Rayleigh scattering regime [25]. The radar system used in this network is called the Weather Surveillance Radar - 1988 Doppler (WSR-88D), sometimes informally referred to as "NEXRAD" (NEXt-generation RADar). Approximately 160 WSR-88Ds make up the operational network in the U.S. The radar was designed to provide quality observations for a variety of meteorological phenomena, from localized intense storms/tornadoes to precipitation events that can cause flooding. The radar also provided improved decision-making for activities such as transportation, aviation, hydrology, and hazardous weather forecasts and warnings.

Severe storms evolve rapidly on timescales of minutes or even seconds in the case of tornadoes [3], [26], [27], [28]. Given the infrequency of tornadoes and other similar phenomena, however, the WSR-88D network was justifiably not designed to provide the temporal resolution that could resolve these rapid-evolving storms. PARs, especially fully digital systems, have the potential of much higher temporal resolution while preserving the required data quality (i.e., bias and standard deviation of radar variables) [29], [30], [31]. This
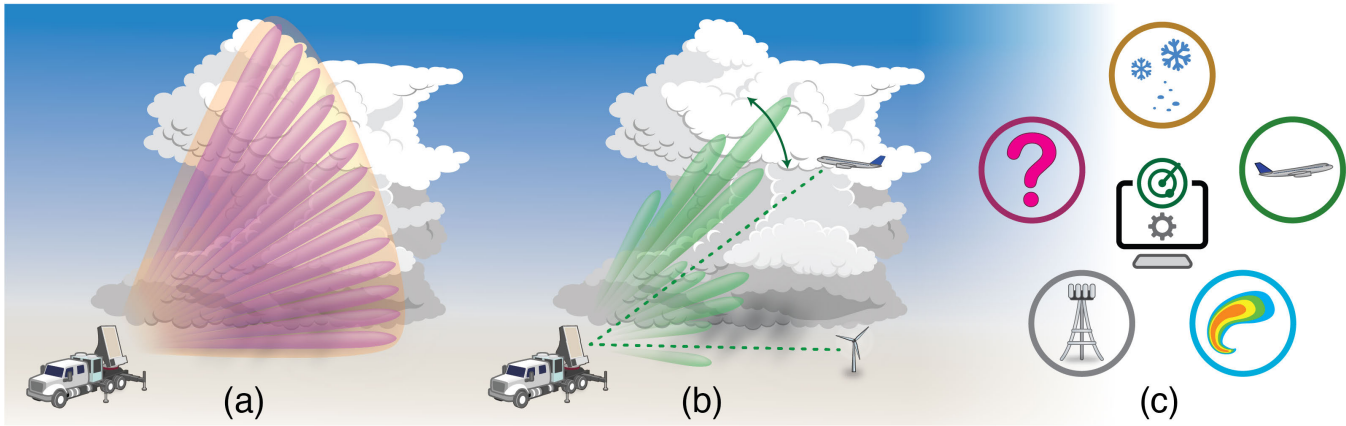
Fig. 2. Artist's depiction of example capabilities of a fully digital phased array weather radar. Shown are (a) dense vertical sampling using imaging in a range-height-indicator (RHI) mode, (b) adaptive nulling for interference mitigation (including non-stationary clutter), and (c) symbolic depiction of software reconfigurability for future requirements/missions.

potential is realized through a variety of advanced scanning concepts that are described later in this section.

In order to achieve adequate angular resolution with a pencil beam, the WSR-88Ds use an 8.5-m parabolic-reflector antenna and continuously scan in azimuth 360° at successive elevation angles. Typically, the number of elevation angles is limited in order to provide reasonable volume coverage every few minutes. WSR-88Ds attempt to cover "full" volumes by repositioning the dish to a limited set of elevation angles (typically 5–15 elevation angles). This imposes an inherent trade-off between temporal resolution, spatial coverage, and data quality. In particular, this limited elevation sampling can leave large unobserved gaps in the measurements, especially at farther ranges. As illustrated in Fig. 2a, one often-overlooked advantage of PARs for weather is the ability of extremely dense sampling in elevation, thus minimizing these observational gaps.

B. Beam Agility and Interference Mitigation

An important capability of fully digital arrays is beamforming flexibility. Since the beamforming weights for each element (and polarization) are realized using software-based digital signal processing (DSP), in contrast to the hardware dependence of analog beamforming systems, it is possible to form multiple arbitrary beams. Examples include spoiled transmit beams with potentially hundreds of simultaneous receive beams (see Fig. 2a). This mode of operation is called "imaging" in the weather radar community [5], [11], [28], [32], [33] and can significantly enhance temporal resolution and vertical coverage at the cost of sensitivity and sidelobe performance. The loss in sensitivity is proportional to the "spoiling factor." For example, if the transmit beam is spoiled by a factor of two, there would be a or the present ponding 3 dB loss in sensitivity. Note that sensitivity may not be an issue in high signal-to-noise ratio (SNR) environments (e.g., intense rainfall, hail, etc.) and can be mitigated through the use of phase-only transmit weights [34], [35], [36], [37]. The two-way sidelobe performance challenge can be addressed by using a "spoiled" transmit beam with multiple lobes spaced in angle [38], [39], rather than a single wide transmit beam. This transmit beam design allows a more effective path to meeting two-way sidelobe requirements since the receive beams are not adjacent in angle.

Of all PAR architectures, fully digital PARs (also referred to as "all-digital PARs") have the most degrees of freedom for adaptive beamforming on receive using methods such as minimum variance distortionless response (MVDR) [40], [41] (see Fig. 2b). These methods are extremely powerful for mitigation of interference, ground clutter, and even non-stationary clutter, such as reflections from wind turbines [42], [43], [44], [45] where the performance of conventional clutter filters is limited. Further generalization of adaptive sensing can be employed through the use of space-time adaptive processing (STAP), which incorporates adaptive waveforms into the beamforming construct [46]. Such adaptive methods intrinsically depend on the received data at each element and are therefore challenged by the need to aggregate the data in a single processing unit for covariance matrix estimation, matrix inversion, etc. Recent work in AI/ML-based methods may hold promise for adaptive beamforming in a computationally efficient manner [47], [48], [49], [50]. Although a burgeoning area, the use of AI/ML methods for a variety of other radar tasks, such as control, scheduling, spectrum sharing, dealiasing, etc. [51], [52], [53], will become extremely important for highly digital PARs.

C. Future Proof - Software Defined Radar

Since each radiating element of a fully digital PAR does not have hardware-based phase shifters and attenuators, such systems are by definition "software-defined radars." In addition to the advantages just mentioned and as illustrated in Fig. 2c, a software-defined radar can more readily be reconfigured for new missions. Examples include array segmentation schemes for multiple missions (e.g., weather radar, air traffic control, communications), implementation of sidelobe canceling channels for improved clutter rejection, or new beam shapes for improved temporal resolution, just to mention a few. In the operational weather radar community, it is envisioned that a replacement of the WSR-88D network will be needed by 2040, with the new system possibly having a lifetime of 30–40 years. It is not possible to predict all the future uses

and/or configurations that the radar will have over the coming decades. Therefore, the software reconfigurability allowed by a fully digital PAR is fundamentally important, potentially resulting in substantial savings in maintenance and operations costs over the lifetime of the radar.

III. CHALLENGES AND POTENTIAL SOLUTIONS

As is the case with all new technologies, challenges do exist with fully digital PARs that should be addressed [21]. Many have potential solutions and/or are topics of active research and development. The most important of these challenges are described below.

A. Calibration - Polarimetric Requirements for Weather Observations

In the early 2000s, dual-polarization was being investigated for improved weather observations. After the success of the JPOLE experiment led by NSSL, the WSR-88D radar network was upgraded with dual-polarization capability [54], [55]. This capability has become indispensable to the meteorological community yielding important radar products such as hydrometeor classification [55] and improved accuracy in precipitation rate estimation, a process that is referred to as quantitative precipitation estimation (QPE) [54], [56].

Useful dual-polarization observations are highly dependent on precise calibration. Although challenging, this level of calibration has been achieved with the WSR-88D radar [57]. In the case of dual-polarization on a PAR, however, the challenge is more complex since the array must meet calibration requirements on potentially hundreds of beams with varying characteristics [16]. A dish radar needs this calibration only for a single boresight beam, whereas a PAR requires a beamsteering dependent calibration [6], [58]. For the Horus radar, calibration is performed in three steps. First, utilizing the system's unique digital-at-every element architecture, a novel 'recursive' far-field calibration was applied. In this scheme, array panels are independently calibrated at short-range using a standard gain horn antenna, thereby increasing signal-to-noise ratio and mitigating multipath contamination and resulting in an initially calibrated array (with uniform amplitude and phase excitations). Second, mutual coupling calibration is applied [59] to correct for element-level amplitude/phase differences that may have occurred from the time the recursive calibration was applied to the radar deployment time. Third, after boresight array calibration is conducted, scan-loss correction for the copolar H and copolar V antenna gains are applied as a function of steering angle. These corrections are derived from Horus element-pattern measurements collected in the ARRC's anechoic chamber. Calibration parameters from the combination of these steps are produced on the fly and applied in real time. Equivalently, one could precompute "calibration tables" (one per electronically steered beam position) and apply them in real time. We note that because Doppler measurements depend only on pulse-to-pulse relative phase changes measured, Doppler estimates are insensitive to PAR antenna-induced biases, and the standard error of Doppler velocity estimates only depends on the radar frequency and

dwell time [25]. Although ground truth near-field data are unavailable at this time (yet forthcoming), measurements suggest that the technique achieved acceptable polarimetric array calibration levels. A more extensive discussion is provided in Section V.

The weather-derived products which drive the requirements for the accuracy of polarimetric measurements are differential reflectivity (Z_{DR}), copolar correlation coefficient (ρ_{hv}), and specific differential phase (K_{DP}). Z_{DR} is the logarithm of the horizontal (H) to vertical (V) returned powers ratio, ρ_{hv} is the correlation coefficient between the H and V returns, and K_{DP} is the derivative of the differential phase (Φ_{DP}) with respect to range; where Φ_{DP} is the phase difference between the returns in H and V polarized waves along a radial up to a specified range. To conduct precise measurements of polarimetric variables, it is crucial that the beams for transmitting the H and V polarized waves are well matched in gain and shape at every scanning direction. To achieve an accurate estimate of rainfall rates, it is recommended that the bias of Z_{DR} estimates is kept within ± 0.1 dB for intrinsic Z_{DR} between 0 and 1 dB and less than $0.1 \times Z_{DR}$ for larger Z_{DR} values [60]. It should be noted that keeping the bias of Z_{DR} estimates within ± 0.1 dB is exceptionally difficult to achieve even in radars with parabolic antennas (e.g., WSR-88D network), and for this reason, the bias accuracy to within ± 0.2 dB for Z_{DR} less than 1 dB (and up to $0.2 \times Z_{DR}$ for larger Z_{DR} values) has been broadly adopted as a calibration goal. In the case of ρ_{hv} estimates, a bias within ± 0.006 is deemed sufficient for "sensing the mixed-phase precipitation and gauging the hail size quantitatively."

Large PAR systems are typically calibrated (e.g., phase/amplitude alignment) using a near-field scanner prior to system deployment. Unfortunately, any changes in the array performance in the field often result in a need for dismantling the radar and recalibration in a laboratory setting. Fully digital PARs have the potential of using the inherent mutual coupling among individual elements to realign the array after being deployed [59]. This solution to the calibration challenge is an important advantage of fully digital PARs. Further discussion on the use of this approach for the Horus system appears in Section V. Recent work has also shown that polarimetric performance enhancements can be achieved with a fully digital array using the so-called cross-polar canceller (XPC) technique [61], [62], [63]. This method assigns a small number of elements from the entire array in an attempt to mitigate cross-polar contamination by transmitting the opposite phase from the original signal.

B. Power Consumption

At a high level, prime power consumption of a PAR system can be segmented into the (1) transmit/receive (TR) modules including the high-powered amplifier (HPA), low-noise amplifier (LNA), and any phase shifters and attenuators, (2) digital transceivers, (3) back-end processors, and (4) off-array computational needs. For a fully digital PAR, every element (and polarization) is digitized and processed, meaning that the digital transceivers and any onboard processing (e.g., FPGAs) dominate the power needs. Of course, onboard

processing results in lower power consumption for off-array computations. Furthermore, fully digital arrays require no phase shifters/attenuators in the TR module. Nevertheless, the prime power needs for a fully digital PAR are certainly larger than for a PAR based on analog beamforming. For example, the power needed for the Horus radar discussed in the next section (assuming 1600 radiating elements) would be approximately 50 kW of prime DC power for the array only. This number does not include the radar infrastructure (e.g., chiller, back-end servers, pedestal, etc.), which can be significant but is independent of the PAR architecture. Fortunately, several efforts are underway in industry to design dedicated application-specific integrated circuits (ASICs) for the digital radar market [64]. In addition to providing the flexibility inherent in a digital array, these new ASIC designs will have the capability to reduce overall power consumption.

C. In-Band Interference

Interference is an important issue for any radar or communication system. Mitigation strategies include filtering, of course, with the goal of rejecting sources outside the operating frequency band. In-band interference can also be an issue, with sources from intentional jammers in defense applications to unintentional interference in all application spaces. A major concern with interference is that the A/D converters and/or mixers in the digital transceivers could become saturated resulting in unusable data. Analog beamforming for either the entire array or at the sub-array level enables some level of angular directivity since the array (or sub-array) pattern will be relatively narrow compared to the radiation pattern of a single element. For a fully digital system, there is little spatial directivity since each element is digitized and the element pattern can be ~40–60° wide [65].

At least two potential solutions for in-band interference of fully digital PARs exist, and precursor systems to Horus have been used to explore these [66], [67]. First, as will be described in the next section, the Horus radar is based on the Analog Devices AD9371 digital transceiver integrated circuit (IC). The AD9371 is a direct conversion receiver [68], [69]; hence this zero-IF downconversion plan provides baseband in-phase (I) and quadrature (Q) digital signals with 16-bit sampling. The dynamic range afforded by this sampling is sufficient to adequately for signals with moderate levels of interference. Moreover, the overall dynamic range of this digital beamforming radar is increased by a factor of $10 \log_{10}(N)$ compared to an analog beamforming radar that uses the same receiver [70], [71]. For Horus, N>1000, and this is especially useful for civilian applications such as weather observations whose echo strengths can span an 80 dB power range [72]. Second, miniaturized frequency-tunable filters are being investigated that could be embedded into the antenna array [73] with little impact on antenna performance. Other more exotic mitigation strategies have also been investigated, such as element-level angular selectivity based on tunable mutual coupling resonant circuits [74].

D. Data

With a rudimentary calculation based on digitizing each element and polarization of an array made up of thousands

Operating Frequency	2.7–3.1 GHz
Element Polarization	ATSR/STSR/RHCP/LHCP
Tx Waveform Type	AWG/LFM/NLFM
Tx Peak Power (single element)	10 W/polarization
Max Tx Pulse Width	100 μs @ 10% duty cycle
Max Tx Bandwidth	100 MHz
Element Spacing	0.5 λ @ 2.951 GHz
Max Number of Panels	25 (1600 dual-pol elements)
Max Electronic Scan Angle	$\pm45°$ az, $\pm45°$ el
Mechanical Positioner	360° az, -1–92° el
Aperture Size	2.03$\times$2.03 m^2
Tx/Rx Beamwidth Broadside	2.58° (no taper)
Total SNR Losses Tx/Rx	6.01/9.81 dB
Sensitivity (1 pulse)	4.3 dBZ @ 50 km

of elements, it quickly becomes obvious that the amount of data is a challenge. For example, a 1600-element Horus radar would produce ~1.5 TB/s at full bandwidth if recording data at each element and polarization and assuming a reasonable received duty cycle. To elaborate, each of Horus' 1600 elements has an independent vertical channel and independent horizontal channel, with each channel possessing its own digital receiver. The AD9371 digital receiver is rated to sample up to 125 MSPS, and each 16-bit sample is mapped into a word of two bytes. Each receiver which produces a unique two-byte in-phase signal and a unique two-byte quadrature signal. Collectively, this produces more than a terabyte of data at full bandwidth, as mentioned above. It should be mentioned that we subsequently govern sample rate of the in-phase and quadrature signals leaving the digital receivers by changing decimation factors and designing decimation filters to produce output data rates that accommodate the next item in our digital chain. On the other hand, analog beamforming systems (and sub-array systems) reduce the number of digitized channels at the expense of flexibility and advanced capabilities. Data reduction on a digital array can be achieved via digital coherent beamforming, which has the advantage of improved SNR since noise from different channels has a lower correlation, while reducing the sheer amount of data for both transport and processing. Various real-time beamforming topologies proposed include systolic schemes and others that will be discussed in the next section. Of course, all methods rely on an efficient data networking system.

IV. HORUS SYSTEM OVERVIEW

The Horus radar, shown in Fig. 1, is an integrated mobile radar system designed to demonstrate the feasibility of fully digital radars and enable research into the opportunities and challenges presented by such designs. As mentioned, the radar system consists of 1600 dual-polarization S-band elements. Each active element is driven by two fully independent radar chains. The high-level specifications of the Horus radar are listed in Table I. To elaborate on this table, conservative loss estimates have been accounted for during the design process, so that the resulting hardware system will perform as expected. For instance, we estimated total transmitter losses of 2 dB, an aperture efficiency of 50 percent, and a TX waveform taper loss of 1 dB; hence, a 6 dB loss on transmit was
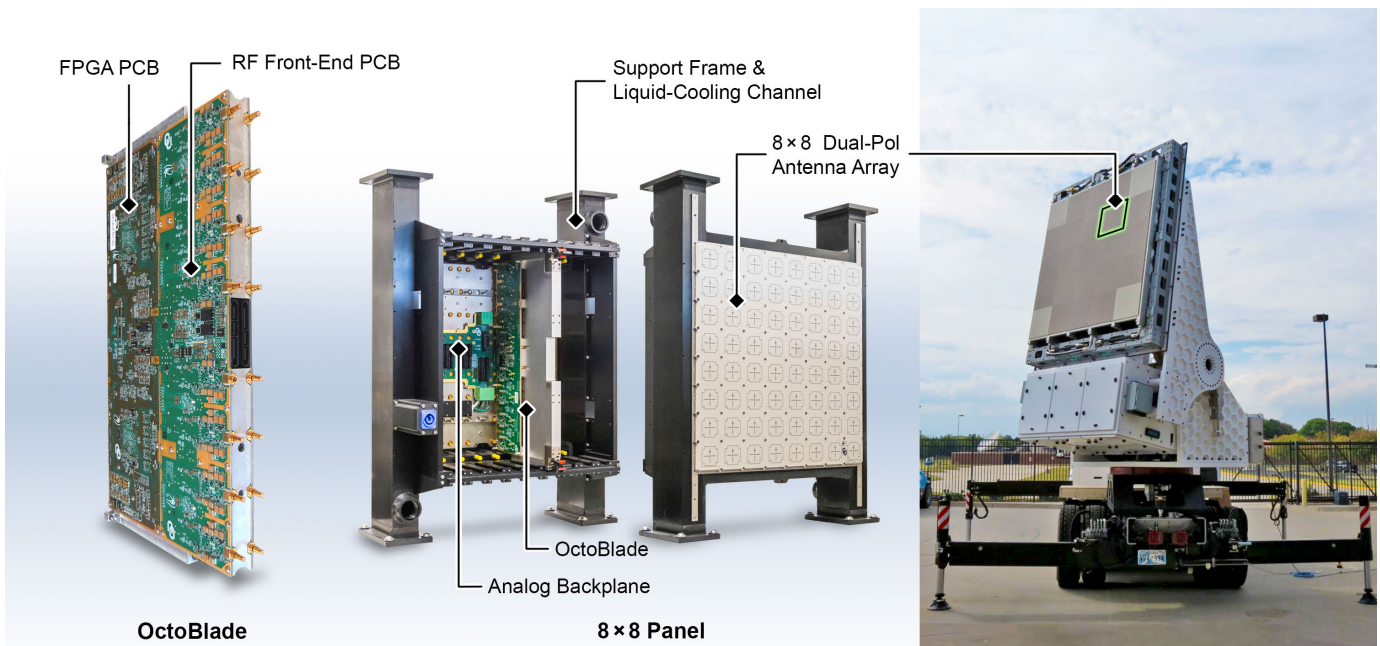
Fig. 3. Photographs of the OctoBlade (left), 8×8 Horus panel (center), and the 25-panel Horus truck (right). The scalability of the Horus design is emphasized with annotations for the subsystems/features of the OctoBlades and the 8×8 panel.

estimated. On receive, our lab data revealed a receiver noise figure of 3 dB, receive antenna losses (elevation scan angle loss 1.5 dB, elevation beamwidth taper loss 1.4 dB, azimuth scan angle loss 1.5 dB, azimuth beamwidth taper loss 1.4 dB), and RX waveform taper loss of 1 dB. Our maximum pulse compression gain is established by the apex of the system's time bandwidth product, 100e-6 $\times$ 100e6 = 10e4, i.e., 40 dB. Next, the following paragraphs and sections continue to build upon the data found in Table I.

The mobile platform is built on an International HV607 medium-duty truck. As mentioned in Section III, one of the challenges with fully digital arrays is power consumption. A power take-off (PTO) generator, driven by the truck engine and capable of providing 150 kW, is integrated into the truck below the chiller on the driver's side. The system is liquid-cooled via a 16.7-ton chiller located behind the truck cab. The pedestal provides mechanical pointing of the array in both azimuth and elevation. It can rotate continuously 360° at 12 RPM in azimuth. The elevation positioning is intended to deploy the array to a configurable elevation tilt and remain at that angle during operations. A rotary assembly is integrated into the pedestal which has an electrical slip-ring, rotary fluid union, and fiber optic rotary joint (FORJ). The pedestal is placed on top of a riser, which elevates the bottom of the array above the chiller when the array is deployed into the operational position. Telescoping outriggers are incorporated into the platform for stability and leveling.

The array and supporting back-end electronics are mounted to the pedestal arms in weatherproof enclosures. The back-end electronics encompass the array AC-DC power supplies, data processing and storage servers, networking, and centralized timing and synchronization electronics. Co-locating the digital array with the back-end electronics simplifies the connections that must be made through the rotary joint and slip rings.

A. High-Level Architecture

Many decisions and technical compromises must be made when developing a complex system such as the Horus radar. System scalability was a key design constraint for the array electronics. Additionally, maintainability and modularity were important considerations during the design phase of the array electronics to ensure the system could be supported for many years, while also offering opportunities to upgrade various aspects of the system during the course of future research.

The Horus panel electronics provide the scalable building block of the fully digital array. The block diagram of a Horus panel for a row of eight dual-polarization elements within the panel is shown in Fig. 4. The antenna for each Horus panel consists of 64 passive radiating elements connected to the RF electronics via SMP-MAX connectors. The antenna mounts to a continuous ground plane from the front of the array, while the rest of the panel electronics are installed from the rear for accessibility during system maintenance. The Horus array electronics utilize a brick architecture to provide a highly serviceable and modular hardware platform. As a ground-based system, there is space for the depth of a "brick" architecture, rather than being constrained to panelization of the electronics in a tile. Since the electronics are not as tightly integrated as required by a tile architecture, the material stack-up and fabrication design rules for each printed circuit board (PCB) in the panel are individually tailored to improve manufacturability and minimize fabrication costs.

A passive backplane for power distribution, known as the Analog Bridge, is installed inside the panel as seen in the center portion of Fig. 3. Eight OctoBlades and a SuperBlade constitute the brick assemblies that populate the array. An OctoBlade contains the full radar chain from the analog RF radar front-ends through the digital transceivers and processing for eight dual-polarized antenna elements.
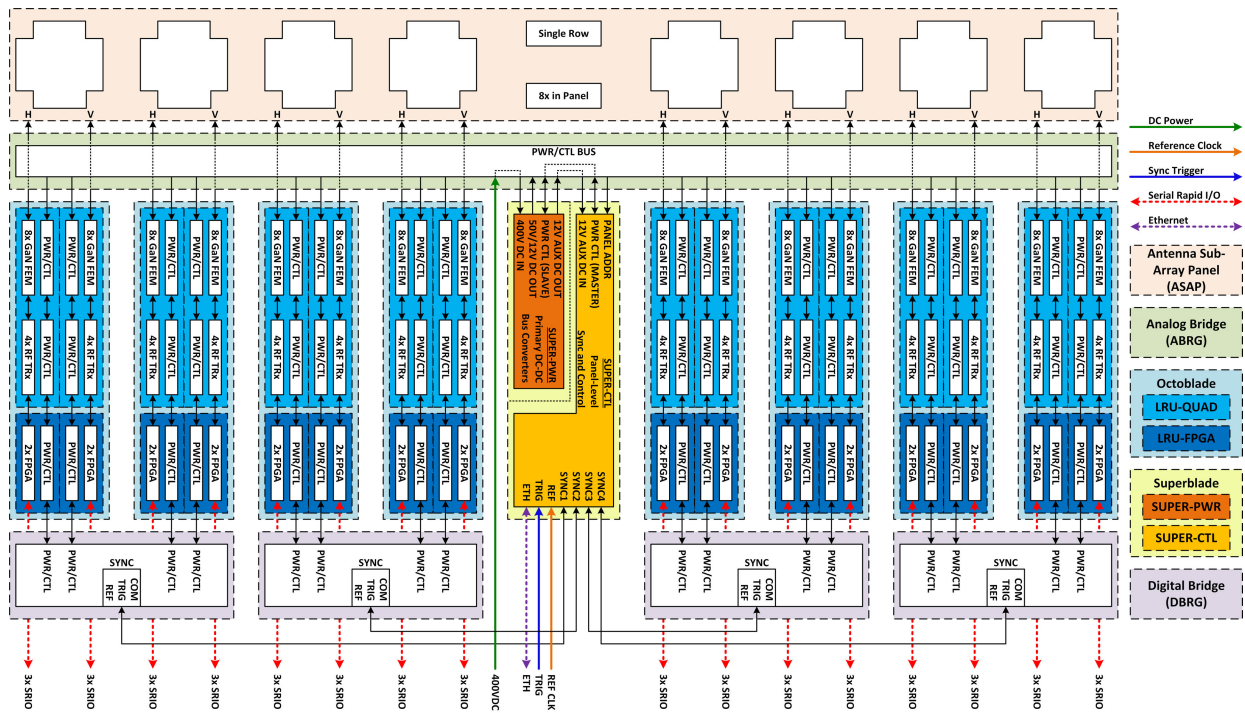
Fig. 4. Block diagram for a row of eight dual-polarization radiating elements within a single Horus panel. The dual-polarization antenna panel is depicted at the top with the so-called Analog Bridge just below. Each antenna element has signal paths to the RF front-end modules and FPGA-based processing boards on the OctoBlades. The bottom of the block diagram represents the Digital Bridge, used for synchronization and timing reference distribution. The SuperBlade is shown in the middle and provides power to all the OctoBlades through the Analog Bridge and synchronization through Digital Bridges.

The SuperBlade is responsible for converting the system-level 400 VDC power to 50 VDC and 12 VDC used by panel electronics, as well as, centralized monitoring, control, and signal distribution for each panel. Digital Bridges span the back of two OctoBlades and assist the SuperBlade with distributing timing, synchronization, and control signals to the FPGA boards within the OctoBlades.

The OctoBlade serves as the fundamental building block of the Horus radar. Given the importance of this line-replaceable unit (LRU), the high-level design of the OctoBlade is described next.

B. The OctoBlade

The OctoBlade is the heart of the Horus panel electronics, containing the radar front-end, RF-to-digital transceivers, and radar signal processing FPGAs. A single OctoBlade supports eight dual-polarization antenna elements with its 16 channels of radar electronics. As with other aspects of the system, the OctoBlade is also modular, primarily to facilitate system upgrades, scalability, and design reuse in future projects. Modularity is also beneficial during volume production for PCB yield rates, as it reduces the number of electronics that must be discarded if there is a PCB that does not pass the quality assurance tests and is unable to be repaired. The OctoBlade, as seen in the left panel of Fig. 3, has three main components: the Quad board (OCTO-QUAD), the FPGA board (OCTO-FPGA), and the Heat Transport Duct (HTD). A single blade consists of an HTD in the middle with a mated set of Quad boards and FPGA boards mounted on either side of the HTD, and a pair of metal lids for enclosure (not shown

in Fig. 3). The two sets of Quad/FPGA boards on either side of the HTD feed eight RF ports for a single polarization. By feeding the antenna in this fashion, the OctoBlade has the benefit of physically isolating the H and V polarization circuitry, which preserves the inherent polarimetric isolation provided by the antenna by minimizing parasitic couplings. The OctoBlade is hot-swappable and is also symmetric, so the OctoBlade is insensitive to orientation when installed in a panel.

The Quad board is responsible for the analog RF circuitry and the conversion between the RF and digital domains. Each of the eight channels on the Quad board has an independent radar chain with a 10 W GaN high-power amplifier (HPA), a transmit and receive switch (T/R switch), a limiter, and a low noise amplifier (LNA). Since Horus is a fully digital radar, digitally controlled stepped attenuators and phase shifters are not necessary, as that functionality is implemented in the FPGA digital signal processing fabric. An attenuated bypass path around the LNA is implemented to enable high linearity measurements of mutual coupling while transmitting full power out of nearby elements to assist with system calibration. The Analog Devices AD9371 is a dual-channel RF transceiver capable of tuning from 300 MHz to 6 GHz with up to 100 MHz of instantaneous bandwidth. This highly integrated transceiver is utilized on the Quad board to provide the translation layer between the RF radar front-end and the digital interface between the Quad board and the FPGA board. The Quad board also incorporates several supporting circuits, like numerous RF calibration paths between the AD9371 and the radar front-end, external LO distribution to the AD9371,

and hot-swap power controllers to protect the Quad board in the event of power issues.

The main processing on the FPGA board is implemented with a pair of Intel Arria 10 GX FPGAs that perform the array signal processing and digital waveform generation. Each Arria 10 is supported by a bank of double data rate version 4 (DDR4) RAM for storing arbitrary waveforms and buffering receive samples prior to digital beamforming. Nowadays, utilization of DDR4 RAM in modern radars that rely on FPGAs [75], [76] is one of the best ways to achieve real-time beamforming and other radar functions at reasonable power and monetary costs. An Intel Cyclone V System-on-a-Chip (SoC) FPGA based daughtercard, running Linux on the hardened ARM processor cores, configures and manages the Arria 10s, the AD9371 transceivers, as well as, performing online diagnostics and ensuring proper operation of the electronics. Four Samtec QRM8-RA connectors provide the JESD20B, SPI and GPIO interfaces for the AD9371 transceivers and for controlling the radar front-end. External LOs for the AD9371s feed through the FPGA board from the Digital Bridge to the Quad board. The data network on Horus is implemented within the Arria 10 FPGAs and exposed via six Samtec ARC6 connectors on the rear of the PCB. These connectors route directly to four high-speed serial transceivers per port on the Arria 10 FPGAs. In addition to the external ports, there is an internal network port between the two Arria 10s routed through the PCB. This implementation is protocol agnostic, enabling the exploration of varying network protocols and architectures. Additional diagnostic interfaces, such as JTAG, I2C and a serial UART console for the Cyclone V SoC, are available to the SuperBlade via the Digital Bridge to support managing and debugging OctoBlades while installed in the radar system.

The HTD is an aluminum cold plate with blind mates to liquid distribution manifolds that are integral to the Horus panel mechanical structure. The internal serpentine fluid path navigates by each of the major heat-producing components on an OctoBlade to move the heat into the coolant. The HTD utilizes Staubli dripless connectors to allow an OctoBlade to be inserted and removed from a panel without leaking, even while fluid is circulating through the rest of the system.

C. Cooling and Structural System

It is important to maintain stable thermal characteristics and minimize temperature gradients across the aperture on phased arrays for system reliability and calibration performance. While the HTD is responsible for removing the heat from an OctoBlade, the Horus system has been designed to appropriately distribute and collect the coolant fluid throughout the array in a practical and scalable manner. When the Horus project first began, air cooling was considered, however, it was determined that while potentially feasible at a single blade level, the necessary amount of airflow and pressures involved were not practical at the system level. As a result, the decision was made to liquid-cool the system.

The fluid distribution for the array is incorporated into the mechanical structure of the panel. The electronics lattice is intentionally reduced compared to the element lattice spacing within the panel, in order to make space for the supporting mechanical frame and fluid distribution. In Fig. 3, one can see the rectangular aluminum columns on either side of a panel that were used during prototyping. Horizontal fluid distribution manifolds are welded between the vertical columns at the top and bottom of each panel. Each horizontal manifold is only open to one of the vertical columns, forcing the fluid to flow through the OctoBlade and SuperBlade HTDs in a panel passing the exhaust fluid through the other horizontal manifold and vertical column. Each horizontal manifold is shared between adjacent panels vertically, alternating the fluid flow direction through HTDs with each panel. Likewise, each vertical column is shared between adjacent panels horizontally across the array. This method of fluid distribution ensures that all HTDs in the system are in parallel and no coolant flows out of one HTD and into another. This results in nearly uniform temperatures across the full array, minimizing thermal impacts on array calibration.

D. Antenna Design and Validation

The Horus antenna design was focused on achieving the same or improved performance compared to that of WSR-88D parabolic-reflector antennas. These design specifications are critical, given that the weather mission presents more challenging polarimetric requirements, in terms of accuracy of estimates than those for aircraft surveillance missions. A Horus antenna panel is composed of 64 elements (8×8) configured in a two-dimensional square lattice of 0.5λ spacing. An aperture-coupled microstrip crossed-patch radiating antenna element with independent feed layers for the H- and V-polarizations was adopted for high cross-polarization isolation (>40 dB) across a scan range of $90°$ in the principal planes [77]. A parasitic microstrip patch layer was incorporated to have a frequency operation from 2.7–3.1 GHz. The antenna array was fabricated using a standard PCB process. Taconic substrate was used for the driving and parasitic crossed patch antennas, and Rogers 4350B was used for the feeding network. Design aspects of the antenna array and scanning performance are presented in [77]. Fig. 5 shows the setup and laboratory measurements. Multiple factors in the antenna element were investigated during the design and fabrication process of the 8×8 array, and these factors include edge diffraction suppression; fabrication tolerances, bandwidth in excess of 15.4% at a central frequency of 2.8 GHz; port-to-port isolation in the element on the order of -50 dB; cross-polarization levels below -40 dB and co-polar mismatch below 0.1 dB at $\pm45°$ and $\pm10°$ for scanning range in the azimuth and elevation planes; and active reflection coefficient of at least -10 dB at $\pm40°$ for scanning range in any plane.

E. Software Architecture

The Horus system is a software-defined radar, which presents many opportunities to develop novel capabilities, along with risks and pitfalls in managing the system complexity and usability. The Horus system is intended to not only be a testbed for advanced fully digital experiments, but
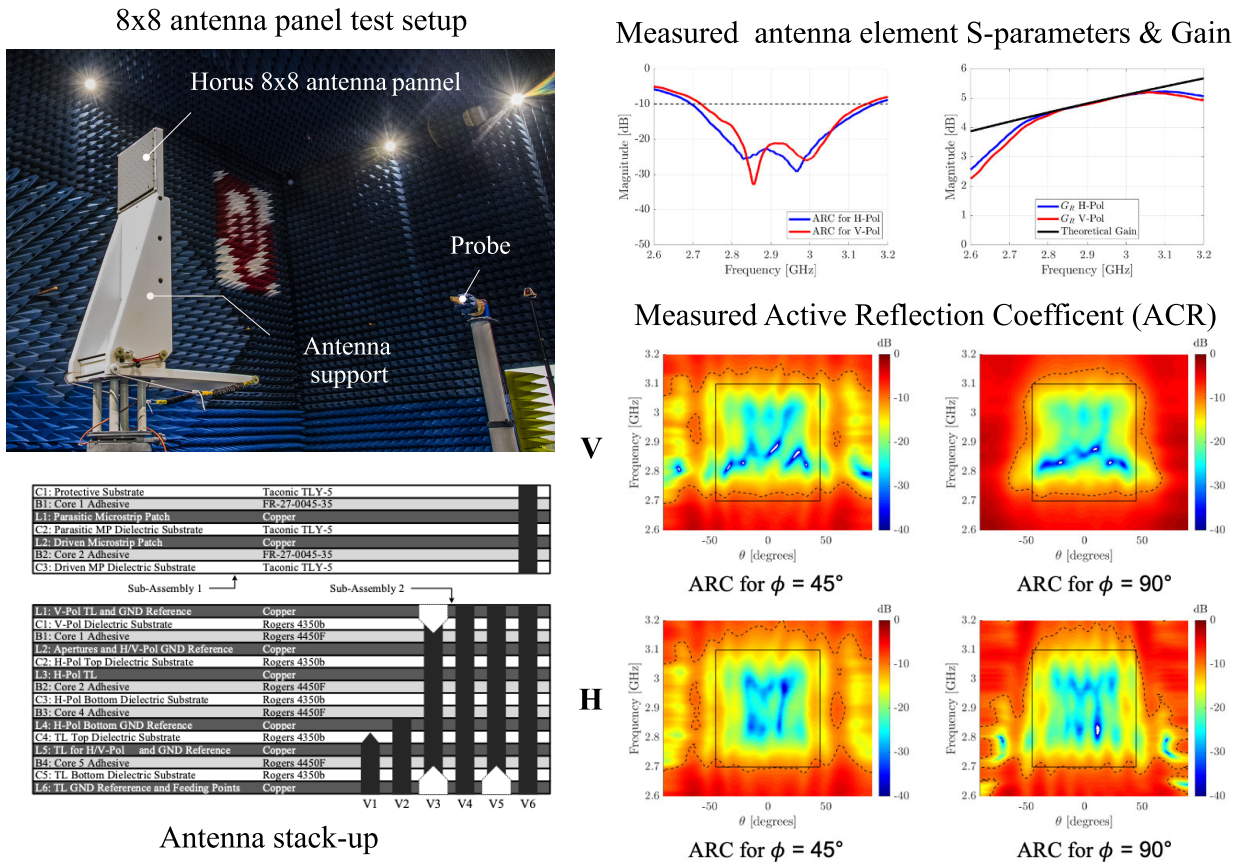
Fig. 5.   Horus antenna panel and measured results. Antenna setup in a far-field anechoic chamber (top-left). Antenna embedded S-parameters (top-right). Measured active reflection coefficient as a function of scanning angle for H- and V-polarizations (bottom-right). Horus antenna stack-up (bottom-left).

also a fieldable system used to routinely collect polarimetric weather data. Significant effort was invested in identifying the most likely deployment scenarios to determine tolerable constraints and assumptions to incorporate into the software, while still enabling many unique capabilities. While this potentially limits certain experiments, the trade-off is rewarded with a substantial improvement in system usability and frees the operator to focus on radar applications rather than radar technology. Since Horus is software-defined, the system will continuously be upgraded to enable new capabilities.

The software is partitioned into four main layers: the deterministic radar signal processing and control in the Arria 10 FPGAs, the embedded software managing the Octo-Blades on the Cyclone V SoCs, back-end data processing on servers and the operator interface running on desktop or laptop computers. Each layer has strengths and weaknesses, progressively trading development ease for performance guarantees as one traverses the layers from the operator interface toward the FPGAs on the array.

The Arria 10 FPGAs define the low-level capabilities of the Horus array, implementing the radar processing chain in fabric. The transmit processing chain in the FPGA encompasses the generation of parametric or arbitrary waveforms, transmit beamforming that applies spatial weights to the generated waveform, transmit alignment calibration to compensate for amplitude and phase offsets between elements, and transmit predistortion to improve system linearity. At the time

of this writing, all of these coefficients are non-adaptive; for instance, the predistortion coefficients are computed offline [78]. On receive, the samples pass through a receive alignment calibration block, down-conversion and decimation to select the desired bandwidth; then the samples are buffered into RAM prior to beamforming. The Arria 10s manage scan scheduling, configuring the appropriate settings for each pulse, and deterministic triggering and control of the functions within the FPGA, as well as, the RF hardware on the Quad board.

To make the high volume of data produced across the array manageable, the conventional Horus operating mode digitally beamforms on the array, so that the data processing servers receive fully formed beams. This enables the reuse of algorithms and processing software previously developed for the ARRC's reflector-based radar systems. Horus currently implements a systolic beamforming architecture over a RapidIO network that interconnects all of the OctoBlades in the array. To elaborate, RapidIO is a commercial open standard interface that supports high-bandwidth, low-latency, packet-switched interconnect between multiple DSP processing elements, and between DSP processing elements and bulk memory. For the Horus team, RapidIO is used to transfer high-speed data between FPGAs for scan configuration and receive beamforming. RapidIO helps to form the distributed backend of the radar. When an Arria 10 receives a packet containing beam data, it retrieves the relevant samples from memory, locally beamforms the directly attached channels, and then

combines it with the data it received. In brief, each of the four Arria 10 FPGAs form weighted sums of the in-phase (I) and quadrature (Q) baseband data that are produced by the four digitizers that precede each FPGA with a partially completed beams from upstream FPGAs; hence, partial beamforming is achieved to reduce the amount of raw I and Q data that need to be routed. Once the FPGA has contributed its data to the partial beam, a packet is sent to the next FPGA to repeat the process until the beam is fully formed and ingested by a server via a PCIe FPGA card connected to the RapidIO network.

Overall, the Horus radar is controlled by a scheduler that can switch among scan strategies on a coherent processing interval (CPI) basis. Generally, the "scan strategy" refers to the pulse waveform, polarization state, transmit/receive beam weights, PRT, CPI, number of beams, etc. Therefore, volumetric update rate can be readily traded with data quality. From a system-design perspective, the Horus software architecture has been designed to provide the user maximum flexibility with the overarching goal of producing the highest temporal resolution possible while maintaining high-quality polarimetric weather radar observations.

V. Calibration

As highlighted in Section III, the technology landscape supporting modern digital arrays has continually maturing tools for establishing and maintaining calibration and alignment as an intimate corollary to their inherent challenges and opportunities, and this concept is explored more broadly in [21] and [79]. For the present work and discussion on calibration, the focus is first and foremost on approaches to maintaining proper alignment, sufficiently low sidelobes, and correcting for polarimetric-measurement errors. For clarity, we cite Patton and Yorinks who describe "alignment" of a phased-array antenna as the process of bringing all of its radiating elements into phase alignment so that their radiated power will add coherently in a given direction [80]. An important note, however, is that the development of this and similar digital array systems allows for the exploration of the practical limitations in digital array calibration that the team has previously studied. This includes quantifying and extending other performance metrics such as dynamic range [67], [81] and spectrum-related interoperability using digital nonlinear equalization (NLEQ) and digital predistortion (DPD) [82], [83] or even intentional decorrelation of spurious products [66] to maximize dynamic range. For example, such relatively low-power spurious products include third order harmonics and intermodulation terms.

Horus has a number of tools from which it can leverage built-in or auxiliary measurements to assess or estimate the element-level amplitudes and phases of the signals on the data converters (ADCs and DACs) *relative to what they should be*, ideally, if the array is scanning (transmitting or receiving) to or from a particular angle. Horus achieves this with a specific overall aperture window or taper, taking all physical effects into account. The techniques being used and explored all seek to assess these *ground truth* relations between the element- (and polarization) - specific digital waveform amplitudes and
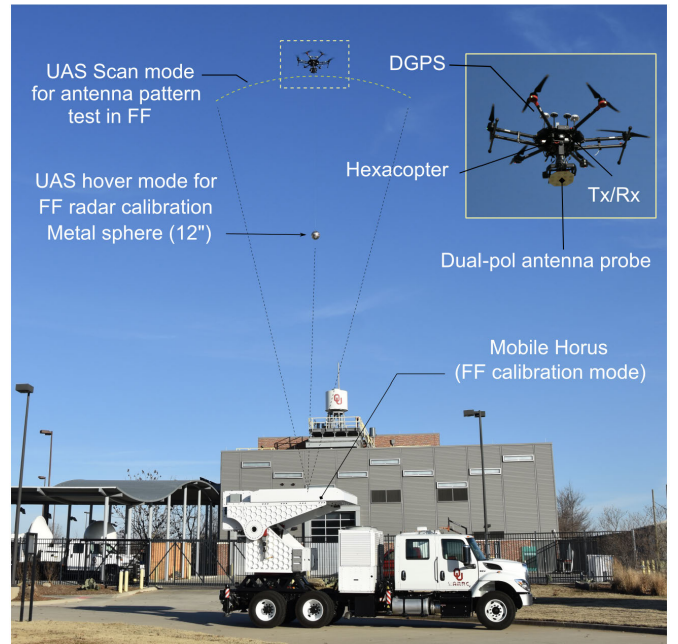

Fig. 6. The Horus radar in bird-bath mode for far-field calibration and antenna pattern characterization. A 12-inch metallic sphere tethered to the UAS platform, in hover mode, is used for radar calibration. The UAS in spherical scanning mode is used to characterize antenna patterns in the far field.

phases and the actual fields that would exist in a clear atmosphere.

For the purposes of discussion, a brief overview of each of the procedures is given next, followed by references to many more fundamental/in-depth explorations.

A. Far-Field Calibration and UAS-Based Measurements

Traditional methods for far-field phased array calibration are extensions of classical far-field measurements [84] to element-level amplitude and phase alignment and/or for assessment of dual-polarization performance [85]. Characterizing antenna patterns with high accuracy typically requires the use of specialized indoor or outdoor antenna range facilities. In both cases, the intrinsic properties of the antenna pattern measurements must exclude undesirable reflections, diffraction, and other external sources of contamination that may influence the overall measurement. When the radar system is deployed, the antenna array is mounted on a mechanical pedestal and is surrounded by other elements such as a radome, tower, lightning protection, and RF equipment. Ground irregularities produced by topography, morphology, and environmental conditions (temperature and humidity) that are different for each site have also been proven to negatively impact the overall performance of radars. Nevertheless, the team has leveraged far-field measurements before for array alignment and calibration [19]. For large arrays, such an approach requires a separation between the radar of aperture diameter D and measurement antenna on the order of $2D^2/\lambda$, which is not practical indoors for S-band weather radar systems.

As an alternative to this traditional far-field measurement, the ARRC team has proposed and demonstrated a
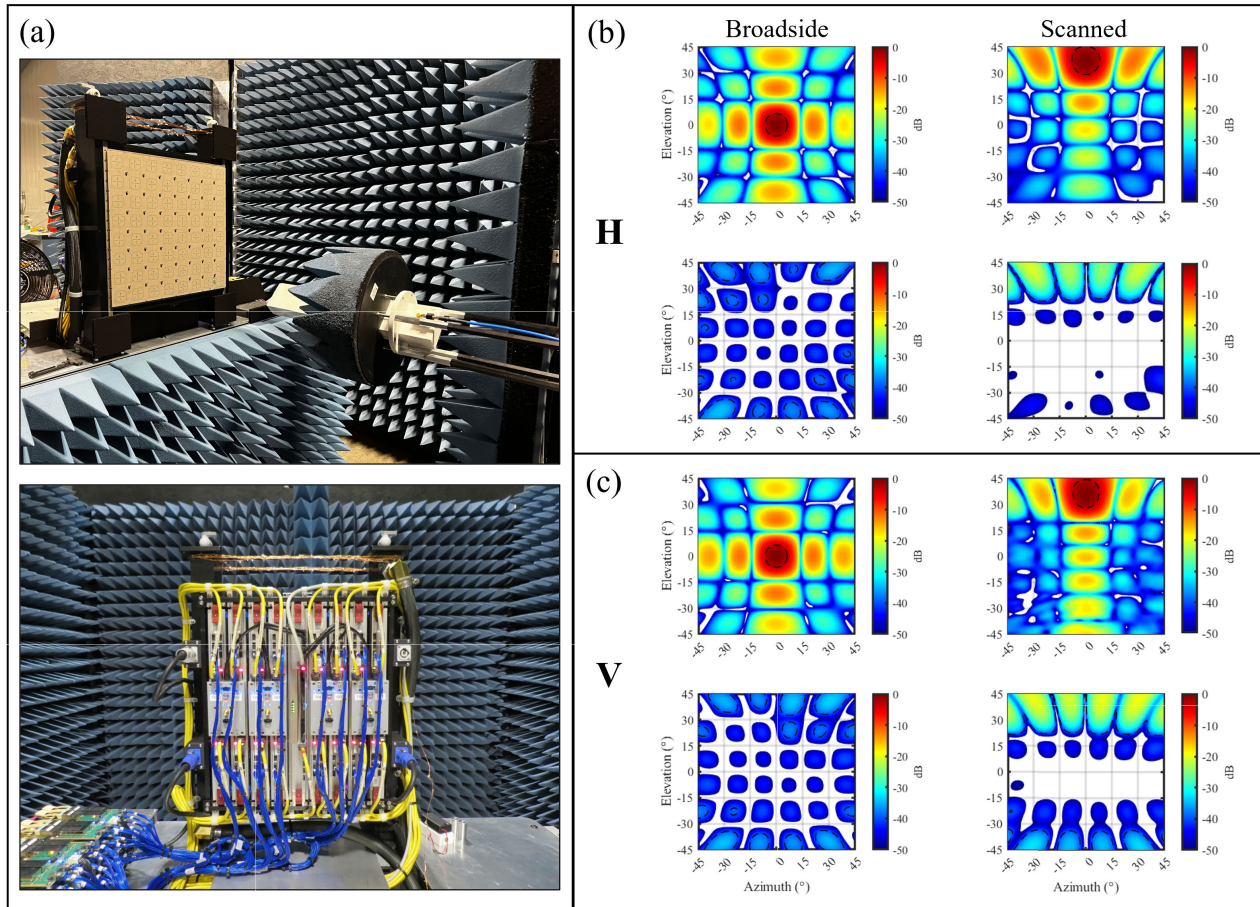
Fig. 7.   (a) Photographs of the near-field scanner setup used to characterize the H and V antenna patterns in the far-field region of the fully active Horus 8×8 antenna panel; (b) The normalized H co-polar (top row) and cross-polar (low row). Horus far-field patterns derived from near-field measurements, with the left column showing broadside beam measurements and the right column showing a beam scanned at 36° in elevation; (c) Same as (b) but for V far-field patterns. Dotted contours on the co-polar H and V patterns indicate the half-power beamwidth (-3 dB), whereas dotted contours in the cross-polar patterns indicate the -40 dB level.

novel method to characterize the antenna patterns of Horus and far-field calibration using an unmanned aircraft system (UAS). The proposed UAS RF test system uses a commercial hexacopter UAS platform, implemented with a customized RF transceiver and antenna probe that provides excellent dynamic range polarization performance [86], [87], [88], [89], [90]. The UAS platform dimensions and features were selected to support RF metrology mission for long endurance, position accuracy, stability, and enough payload to carry out an RF transceiver, DGPS system, and RF probe [91], [92], [93].

Fig. 6 illustrates such a UAS-based polarimetric calibration and characterization of the mobile Horus radar. A 12-inch (0.3049 m) diameter metallic sphere tethered to the UAS platform is used to perform a polarimetric radar calibration in the far-field region (>80 m). In this case a separation of 20 m. from the UAS to the metallic sphere is used to minimize the back-scattering contamination from the drone. The UAS in spherical scanning mode is used to characterize antenna patterns in the far field. For antenna pattern characterization, an antenna probe was designed with high polarization isolation (<50 dB) and beamwidth (<40°) to minimize scattering fields induced in the drone [92]. Antenna patterns of the Horus

mobile radar are obtained using a spherical scanning mode when the radar is looking up. This test procedure reduces ground and clutter contamination.

B. Near-Field Calibration

For most large arrays, near-field (NF) measurements provide the standard mechanisms to carefully assess the array characteristics. This is especially true for determining sidelobe levels and pointing accuracy, among other important characteristics. If performed carefully, NF measurements can provide an understanding of root causes of any antenna limitations [94], [95]. For the Horus system, the early work reported in [96] and [97] has continued with a summary included here.

As an initial calibration step, one 8×8 antenna subarray panel of the Horus array was fully populated with electronics that make up the transmit and receive signal paths. The complete subsystem was mounted in a near-field chamber for testing (see Fig. 7a). The near-field scanner is comprised of two motorized Velmex BiSlide assemblies, one Velmex VXM Stepper Motor Controller, an S-band open-ended rectangular waveguide probe (OEWP), a Newport "optical breadboard" base, and RF absorber. These features enable the measurement of antenna patterns for H and V polarizations.

The current process for Horus near-field calibration uses a park-and-probe technique to measure amplitude and phase at each channel. Then, the alignment weights are generated, applied digitally, and verified. Measurement of a full, dual-polarimetric transmit or receive pattern requires four separate data collections, one for each combination of array polarization and OEWP orientation (0° or 90°). The 8 × 8 panel hardware can receive both polarizations simultaneously and feedback the data separately. Multiple beam angles can be collected simultaneously on receive. Up to 16 beams can be formed sequentially. After applying the park/probe and the back-projection calibration methods [97], [98] on the 8 × 8 subarray, the near-field patterns were measured and transformed into the far field.

Normalized copolar and cross-polar H and V far-field patterns are presented in Figs. 7 (a) and (b). The left column shows broadside beam measurements and the right column shows a beam scanned at 36° in elevation. Dotted contours on the copolar H and V patterns indicate the half-power beamwidth (-3 dB) whereas dotted contours in the cross-polar patterns indicate the -40 dB level. A qualitative comparison of the broadside patterns shows excellent mainlobe agreement between the H and V polarizations. The sidelobe structure for each polarization appears to be symmetric about the mainlobe for the horizontal and vertical cuts. Cross-polarization levels are below -50 dB at the peak of the corresponding copolar patterns, and generally going from -55 to -45 dB across all angles. Achieving cross-polarization levels below -45 dB was one of the key goals in the design of the Horus antenna, given the importance of minimizing this contamination for accurate polarimetric measurements [56], [60], [99], [100], [101]. A deeper investigation of polarimetric Horus calibration as a function of beamsteering angle is ongoing; research results will be presented once the investigation is complete.

C. Mutual Coupling

The ARRC team has been exploring and using the ability of highly digital arrays to leverage inherent inter-element mutual coupling measurements to provide feedback paths that encompass the individual phase and magnitude errors of the transmit and receive element's electronics. This concept, which has been used since the early days of such systems [102], is useful for initial calibration and alignment (without the use of near- or far-field test equipment) [103] and in-situ realignment and enforcement of new weightings [19] in digital array systems. Recent activities have been summarized in [96].

As part of the current work, an experiment was designed to measure relative performance of reference-based mutual coupling. A calibration horn was placed in the array's near-field and connected to an optical delay line (ODL) repeater. By transmitting toward the horn from a single array element and receiving time-delayed returns from all array elements, relative alignment was established. Aligning the array using this test setup effectively focuses the array towards a fixed point in space some distance from the array face, and provides a repeatable calibration "target" which can be returned to for validation.
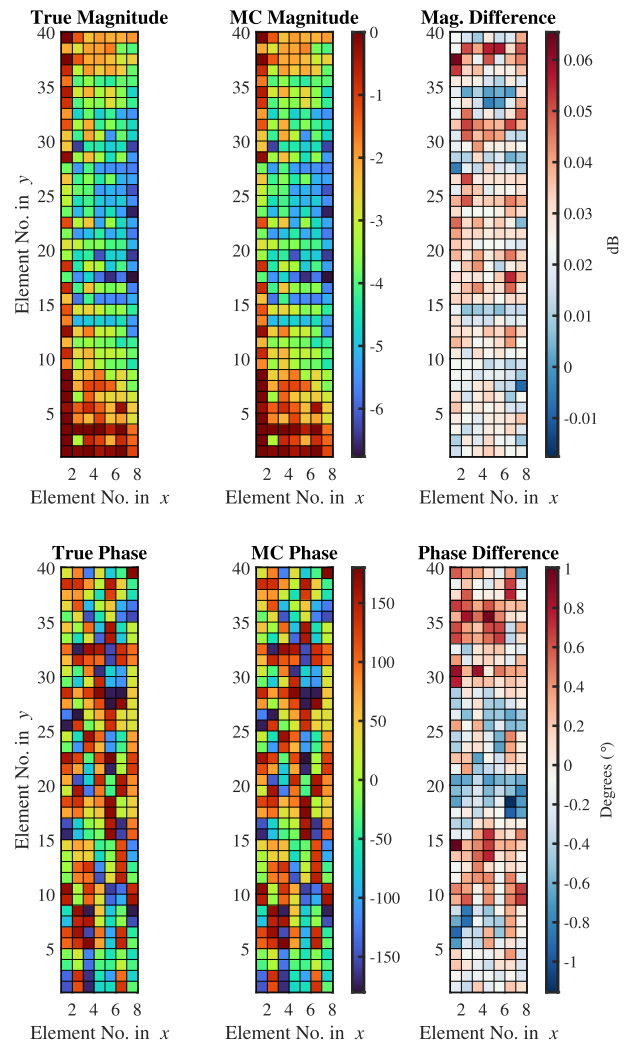

Fig. 8. (upper panels) From left to right, the original magnitude state of the array, estimated magnitude using mutual coupling after power cycling, and magnitude difference with a standard deviation of 0.012 dB. (lower panels) Same as the upper panels, except for phase. In this case, the standard deviation is 0.395°.

Fig. 8 shows one set of results from these experiments. The upper and lower panels show the array magnitude and phase, respectively, for the 5 × 1 array of panels (320 independent, dual-polarization radiating elements) that were populated with electronics at the time of the experiment. The "True Magnitude" provides the magnitude of the ground-truth alignment weights from the experiment described above. The organized pattern seen in the magnitude data results from the actual antenna pattern of the horn. The "MC Magnitude" provides weights estimated based on inter-element mutual coupling. With the array uncalibrated, mutual coupling calibration was applied targeting the "focused" array state, which produced an accurate estimate of the "True" weights. The difference between the truth and the estimated magnitude is provided in the right panel and has a standard deviation across the array of 0.012 dB. The lower panels are equivalent except for phase across the 320 channels. The standard deviation, in this case, is 0.395°.

Although just one example, the results in Fig. 8 illustrate how mutual coupling can be used to realign the array to an
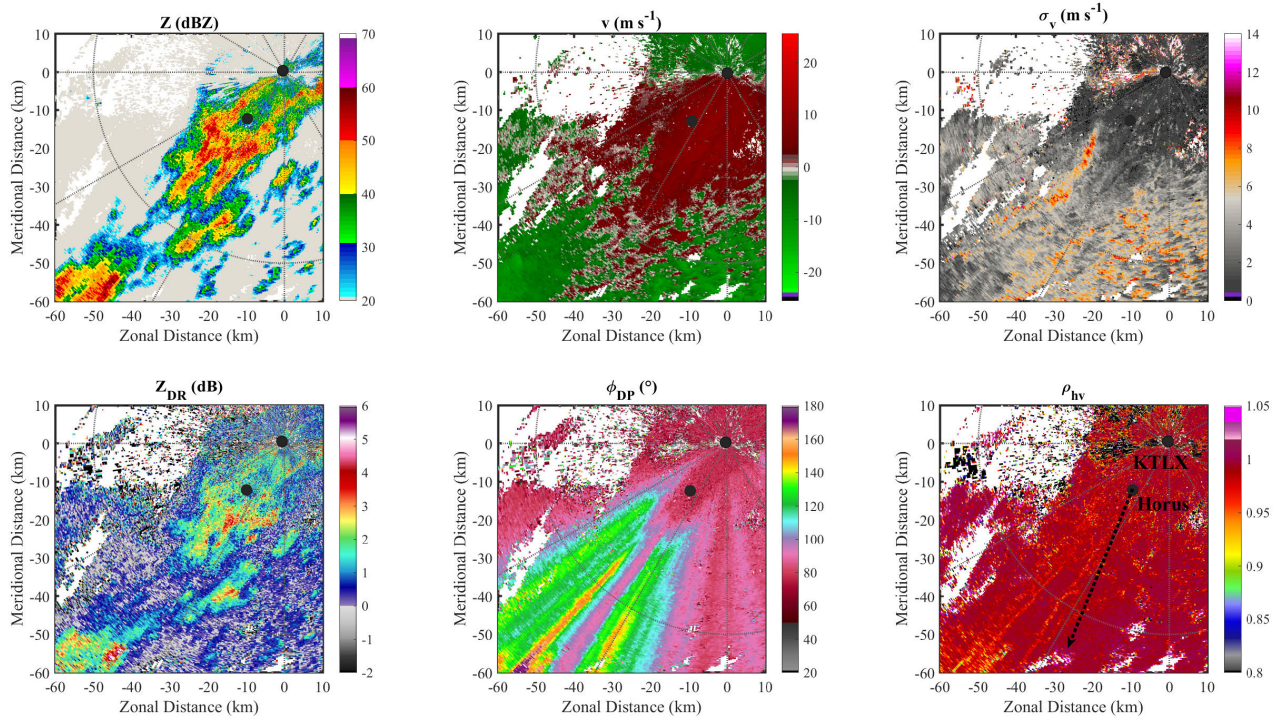
Fig. 9. KTLX Data: Radar reflectivity (top-left), Doppler velocity (top-center), spectrum width (top-right), differential reflectivity (bottom-left), differential phase (bottom-center), and correlation coefficient (bottom-right) fields of data collected by the operational KTLX WSR-88D in Twin Lakes, OK, at 20:35:06 Z on 23 March 2023. These are from the 0.5°-elevation PPI scan. Black circles represent the location of KTLX and Horus, where KTLX is in the origin of the polar coordinate system (see ρ_{hv} panel). A dotted black line in the ρ_{hv} panel indicates the azimuth direction corresponding to the Horus RHIs in Fig. 10.

arbitrary array state. Current work is underway to implement initial array alignment without the need for near- or far-field systems. Such an algorithm would rely on the inherent redundancy in the array geometry and mutual coupling.

VI. INITIAL WEATHER OBSERVATIONS WITH HORUS

A. Meteorological Conditions

During the afternoon of 23 March 2023, a mesoscale convective system formed along a cold front moving West to East over the southern US Plains. Forecast soundings suggested favorable deep shear for supercells (i.e., tornado-producing storms), with intense (25-35 m/s) winds in the 400-mb layer contributing to effective-shear magnitudes in the 30 m/s range. Temperatures changed throughout the day from ~10° C to ~20° C, with similar changes in dewpoint, producing convective available potential energies (CAPE) around 2000 J/kg in central OK. This environment resulted in several storms that produced damaging winds, lightning, hail, and heavy rain from NW Texas into central Oklahoma, as reported by the U.S. National Weather Service (NWS).[1] Many severe thunderstorm and flash flood warnings were issued by the NWS forecasters throughout the event. Fig. 9 shows the radar reflectivity and Doppler velocity fields of data collected by the operational KTLX WSR-88D in Twin Lakes, OK, at 20:35:06 Z. Data are from a plan-position indicator (PPI) scan at the 0.5° elevation. Polarimetric weather data were collected with the Horus radar simultaneously to evaluate initial polarimetric calibration and system performance. The radar was deployed at the Radar

Innovations Laboratory in Norman, OK, from approximately 17:06:22 Z to 21:12:40 Z.

B. Experimental Radar Configuration

Due to the availability of tested OctoBlades, these initial weather observations were conducted with only a partial array of one complete column of panels, forming a 5×1 array of panels (320 independent, dual-polarization radiating elements). The half-power beamwidth of this configuration is approximately 13° in azimuth by 3.1° in elevation. The radar was configured to scan in the range-height indicator (RHI) mode from 0.5° to 32.5° with 0.5° sampling. A pulse-repetition time (PRT) of 1 ms with 64 samples per dwell was used, resulting in a scan time of 4.096 s. Pulse compression waveforms with non-linear frequency modulation were used, with a pulse width of 80 μs and a bandwidth of 5 MHz [104], resulting in a range resolution of 30 m. The progressive pulse compression technique [105], [106] was implemented to mitigate the pulse-compression blind range. Range-time samples were produced at a rate of 15.625 MSPS, resulting in a range sampling interval of approximately 10 m. Data were collected for a range from 0.5–100 km for approximately 10 minutes pointing the antenna broadside to 205° azimuth, scanning the evolving storm cells as they moved toward the radar.

A single beam was formed by the real-time digital beamforming network and the time-series in-phase and quadrature (I/Q) data were processed. The weather signal processor includes several methods to improve data quality, like, spectral-based noise estimation [107], electromagnetic
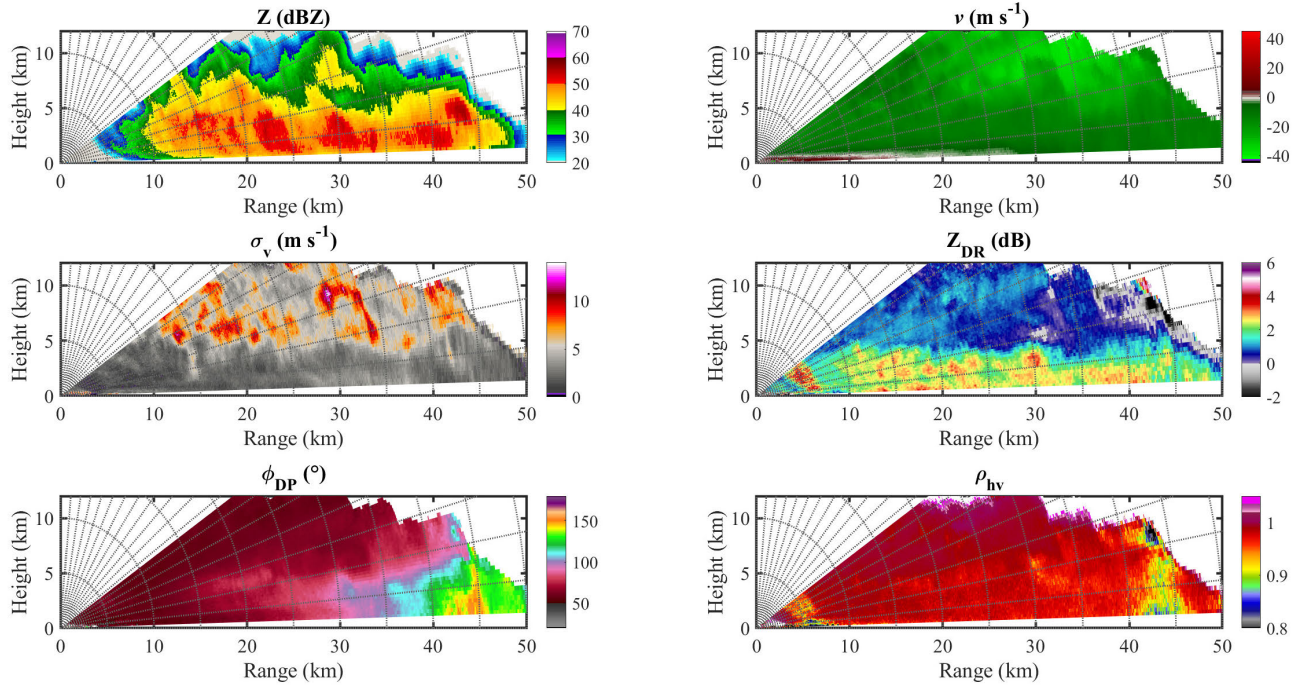
---

[1]SPC: https://www.spc.noaa.gov/exper/archive/event.php?date=20230323

Fig. 10. Horus Data: Polarimetric fields obtained with the Horus 5 × 1 panel array at about 20:35:03 Z on 23 March 2023. The RHI scans are from 0.5° to 32.5° elevation, with sampling of 0.5°.

interference filter [108], ground-clutter filtering [109], and multi-lag estimation [110], [111]. Fields of radar-variable estimates resulting from processing the data from the scan at 20:35:03 Z are presented in Fig. 10.

C. Data Quality Discussion

A qualitative evaluation of fields in Fig. 10 indicates that data were coherently received and processed, since they are relatively smooth and have realistic values. First, the Z_h field shows smooth transitions from lower reflectivities of ~20 dBZ around the edges of the storm, to reflectivities of up to ~55-60 dBZ at certain convective cores within the storm. This follows a conceptual model of the physics of storms, whereby stronger updrafts near the core produce larger concentration and size of hydrometeors increasing the overall reflectivity. Next, the field of v_r shows smooth variation with outbound velocities (red colors) near the surface, and relatively high inbound velocities (green colors) aloft. The transition in Doppler velocity estimates at approximately ~500 m going from outbound to inbound through an iso-Doppler level (grey tones) indicates a smooth change in the direction of the wind field. This is typical in convective storms and represents a change in storm advection direction. Doppler spectra from a location with weather returns of high signal-to-noise ratio (SNR) is presented in Fig. 11, showing the approximately Gaussian shapes of the H and V spectra [25]. Further, the spectra have similar shapes implying good matching of H/V beam patterns, and indicates reasonable polarimetric calibration.

The fields of Z_{DR} and ρ_{hv} in Fig. 10 present relatively smooth changes and plausible values. Specifically, Z_{DR} values are mostly between 0–3.5 dB. Lower values (near 0 dB) are expected at the higher levels of the storm or in regions
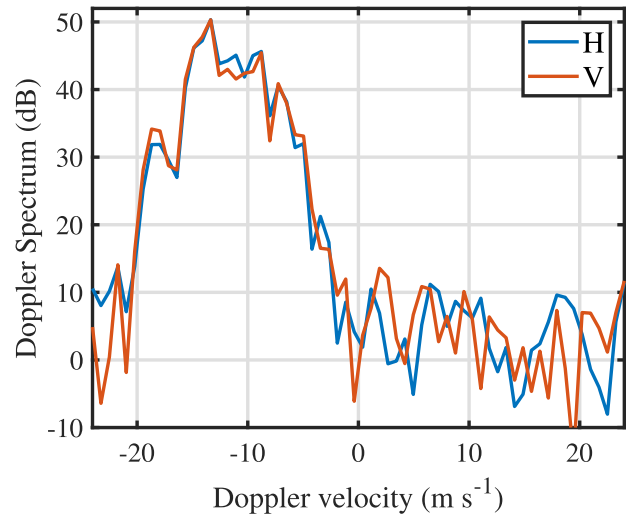

Fig. 11. Doppler spectra from a location with weather returns of high signal-to-noise ratio (SNR). Note that the spectra have similar shapes, which implies good matching of H/V beam patterns, and indicates reasonable polarimetric calibration.

with low Z_h, indicating presence of small nearly-spherical raindrops, or small, randomly oriented ice particles (e.g., crystals, snow) when above the atmospheric melting layer. At lower heights, Z_{DR} is larger as the process of collision/coalescence [112] increases raindrop size and due to air drag force raindrops become oblate as they are falling. This increases the Z_{DR}, which explains the larger values (1–3.5 dB) at lower altitudes. Certain regions of high Z_{DR} coincide with regions of high Z_h, typically observed in the storm updrafts' region where larger (and more oblate) raindrops are present,
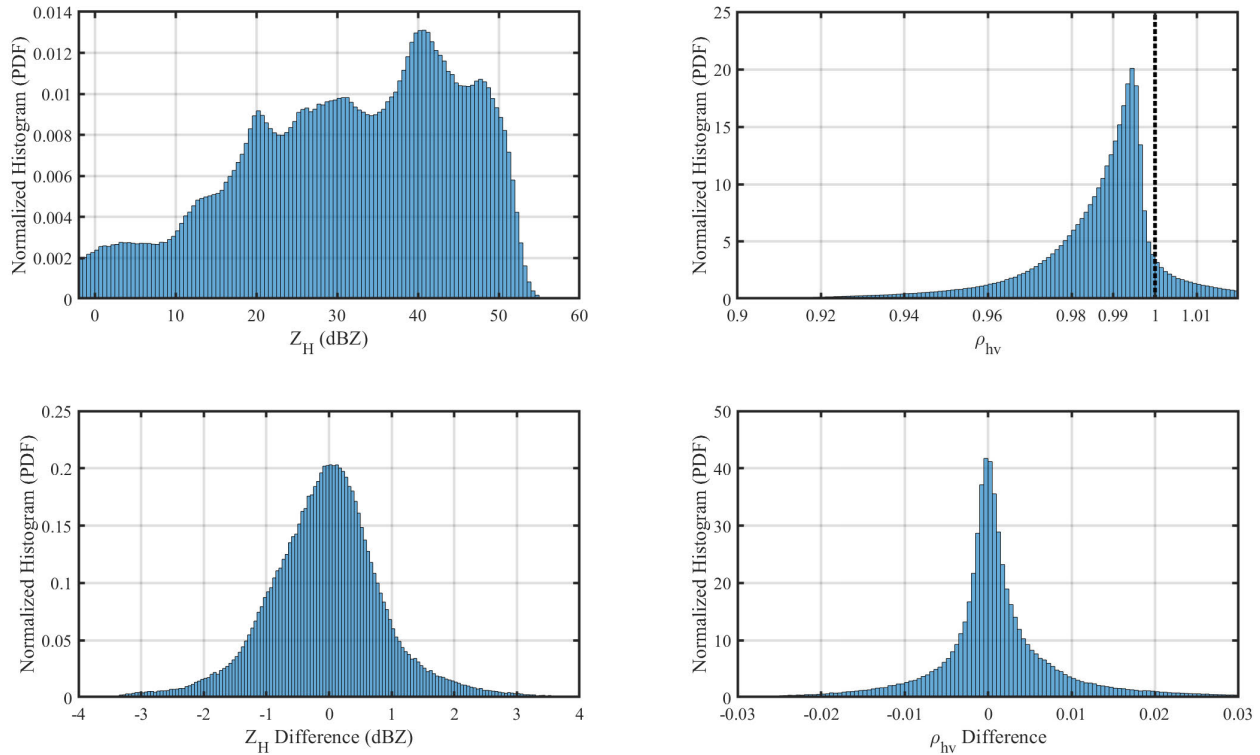
Fig. 12. Histograms of Z_h and ρ_{hv}, as well as histograms of differences between fields of Z_h and ρ_{hv}. (a) shows a smooth histogram of Z_h values; (b) shows the histogram of ρ_{hv} values, where most values are concentrated from about 0.97 to 1, with the peak at approximately 0.99; (c) and (d) are histograms derived using the first ten scans, whereby weather data from the first five scans are averaged and subtracted from averaged weather data from the 6th to 10th scans, and censoring data with SNR $\leq$ 15 dB.

for example, that approximately along the 30 km range and 3 km height.

The magnitude of the correlation coefficient between the horizontally and vertically polarized returns, ρ_{hv} is a key parameter defining the quality of polarimetric radar measurements [113]. The ρ_{hv} field in the bottom left panel of Fig. 10 shows relatively high values (∼0.9–1) as expected from hydrometeors [54]. Most values are approximately 0.99, representing pure water raindrops. The standard errors of the estimates of polarimetric variables are significantly reduced if the maximum ρ_{hv} of the weather signals exceeds 0.99 – a basic requirement for polarimetric weather radars. A region of lower ρ_{hv} is observed at approximately between 40 and 46 km range, where a vertical column with $\rho_{hv} \approx 0.92$ is present. This may indicate presence of mixed-phase precipitation, possibly a combination of raindrops and small hailstones, coupled with some signal attenuation (likely higher in the H polarization) as the has beam propagated through strong precipitation cores. Although this was not confirmed by in-situ instrumentation, it is consistent with the conceptual model of deep convective storm cells. We note that several hail reports were received by the NWS and are available online.

The ρ_{hv} is defined as the normalized absolute lag-0 cross-correlation estimate, i.e., $|\hat{R}_{hv}(0)|/\sqrt{\hat{S}_h \hat{S}_v}$. At low SNR regions, estimates have high standard deviation, therefore, the geometric mean of signal power estimates may be larger than the lag-0 cross-correlation, i.e., $\sqrt{\hat{S}_h \hat{S}_v} > |\hat{R}_{hv}(0)|$, which results in $\rho_{hv} > 1$. Notice that $\hat{S}_h$ and $\hat{S}_v$ are also estimates that

depend on the noise power estimate. Correlation coefficient estimates larger than one are typically present on the edges of the precipitation, far from the radar where the SNR is low and are considered *invalid*. This is commonly observed on ρ_{hv} estimates from any polarimetric weather radar, including those from the operational WSR-88D [114].

Accurate measurements of ρ_{hv} are crucial for polarimetric detection of the melting layer and determination of its height [115] and for identification of the areas with hail and quantification of its size [116]. Therefore, the requirements for the ρ_{hv} measurements in the design of the radars for weather observations are very strict and important. A more detailed evaluation of the impacts of the Horus antenna on ρ_{hv} estimates can be found in [101].

Data from a sequence of 352 scans were analyzed and these showed a smooth evolution of the discussed fields. The scan time series exhibited natural meteorological features consistent with storm evolution and advection, indicating that the Horus data appear accurate and therefore a fully digital PAR technology may be suitable for polarimetric weather observations. To quantify the quality of polarimetric Horus data, we produce histograms of Z_h and ρ_{hv}, as well as histograms of differences between fields of Z_h and ρ_{hv}. These are shown in Fig. 12. Histograms of Z_h and ρ_{hv} are computed using data from the first 60 scans (∼4 min) and include approximately 10 million points. Data censoring is applied using SNR thresholds of 5 dB for Z_h and 15 dB for ρ_{hv} [117] to reduce the impact of measurement noise on polarimetric-variable estimators.

A qualitative analysis of Fig. 12(a) shows that reflectivity values measured were between approximately -2 dBZ up to 55 dBZ. The histogram looks smooth reflecting the expected dependence of returns from precipitation systems (i.e., these usually do not have sharp gradients). The ρ_{hv} histogram in Fig. 12(b) shows that most values are concentrated between about 0.97 and 1, with the peak at approximately 0.994. This is a key indicator of the quality of polarimetric calibration and beam matching, and indicates that Horus can measure the correlation coefficient of raindrops with accuracy exceeding the requirements. Histograms in Fig. 12(c) and Fig. 12(d) are derived using the first ten scans, whereby data from the first five scans are averaged and subtracted from averaged data from the 6th to 10th scans, and censored with an SNR $\leq$ of 15 dB. Resulting difference histograms have zero-mean approximately Gaussian distribution, which is expected, and with relatively narrow standard deviations. The standard deviation of Z_h difference histograms is 0.7824 dBZ and the one for the ρ_{hv} difference histograms is 0.0057. These are within the NOAA/NWS functional requirements for the future operational U.S. weather radar [118], which are 1 dBZ for Z_h and 0.006 for ρ_{hv}.

VII. Conclusion and a Vision for the Future

A. Perspective on Fully Digital Arrays

The authors have attempted to convey the potential of fully digital phased array radars, in general, and more specifically for weather observations. The high temporal resolution afforded by phased arrays is necessary to unravel processes in severe storms, tornadoes, and other high-impact events. In addition to rapid beam steering, fully digital arrays are highly agile in terms of angular sampling and general beam shaping. For example, these sophisticated radars have the potential of creating adaptive nulls on receive with unprecedented degrees of freedom for interference and clutter mitigation. This application is particularly important for moving clutter, such as that caused by wind turbines. As previously emphasized, fully digital arrays are uniquely designed as "software-defined radars," and therefore minimize obsolescence concerns with the ability to reconfigure the array for future and yet-to-be-defined missions. This quality of being "future proof" has the potential to reap a significant reduction of overall operation and maintenance costs over the lifetime of these sophisticated instruments. Although a digital-at-every-element architecture offers extreme flexibility, several disadvantages were noted in Section III. Examples include power consumption of analog-to-digital converters at every element; a significant amount of digital data that needs to be routed; clock synchronization at each data converter must be carefully maintained, and high cost that is sometimes mitigated by subarraying.

In collaboration with NOAA's NSSL, the ARRC has developed the fully digital Horus phased array weather radar. This polarimetric, S-band radar became operational in late 2022 with the goal of demonstrating the potential of fully digital arrays for weather applications. Of particular note for weather observations is the strict requirement for polarimetric

quality similar to the WSR-88D dish-based weather radars operated by the U.S. NWS. It is well understood that the combination of radar polarimetry with phased arrays is arguably the most difficult challenge presented by the technology. Fortunately, the Horus system has been shown to meet this challenge through advanced mutual-coupling-based calibration methods, which should be emphasized are unique to fully digital arrays. For the first time ever, fully digital phased array weather radar data were obtained in December 2022, when the Horus system was deployed near Norman, OK. These initial experiments have shown promising results from a polarimetric quality and beam agility standpoint.

B. Future R&D

Without question, the near-term priority for the Horus radar will be extensive observations with a complete array of electronics. The initial measurements are promising but did not exercise the full capabilities of the Horus radar. For example, only electronic steering in elevation has been attempted thus far. Future experiments will emphasize atmospheric phenomena under a variety of weather conditions, from winter precipitation to deep convection in the spring storm season, utilizing the full capabilities of Horus and showing the potential for scientific novelty. Other non-weather targets of interest include wind farms, wildfires, space debris, aerial biota, and various aircraft (e.g., airplanes, drones, etc.). Convergent research through combined Horus measurements with data from other observation platforms such as rapid-scan satellite radar data will be explored for the study of atmospheric phenomena with multi-frequency and multi-viewing angle observations from ground and space. For example, fast scanning is essential to maximize the collection of matched space-ground precipitation observations for structure and microphysics studies with the Ku/Ka-band PAR radar onboard the Global Precipitation Measurement mission. The future INCUS (Investigation of Convective Updrafts mission) mission will target convective storms and associated fluxes with quickly repeated Ka-band radar measurements that can be compared with their ground-based counterpart to address 2017 Earth Science Decadal Survey key objectives laid out by the National Academies of Sciences, Engineering, and Medicine. The EarthCARE (Earth Clouds Aerosol Radiation Explorer) mission will also carry a W-band Doppler radar that will provide highly complementary observations of precipitation fluxes to Horus. When appropriate, data sharing will be emphasized, especially when engaging the scientific community.

High-quality polarimetric weather measurements rely on accurate and robust array calibration. In early 2023, the ARRC will be finalizing the installation of a large near-field scanner that can be used for array alignment and calibration. These "ground-truth" data will allow accurate beam steering and polarimetric measurements. They will also allow a full-scale demonstration of mutual-coupling realignment, which is vital when considering larger systems. Other important demonstrations will include data throughput capacity, susceptibility to in-band interference, and power consumption measurements. In these cases, theoretical studies have already been performed but validation measurements are prudent.

Other longer-term concepts exploiting the fully digital Horus radar include adaptive beamforming on receive, based on traditional methods and potentially on AI/ML algorithms. In addition, the authors have extensive interest and experience in passive, multi-static measurements for atmospheric observations [119]. To date, these measurements have relied on the WSR-88D radar as the transmitter of opportunity. Certain advantages of using PARs as the transmitter (e.g., mitigation of two-way sidelobes) have been theorized in the past, but not yet demonstrated [120]. Data reduction ideas, such as sparse arrays and various compression methods will also be considered and demonstrated.

Finally, the inherent panel-level scalability of the Horus radar should and must be exploited in the future. Given the S-band wavelength of Horus, even a fairly large array (e.g., 1600 radiating elements for the current system) presents an unacceptable beamwidth for operational radar networks and research applications. By creating a larger array superstructure, tower, power source, etc., a fully digital, S-band, phased array weather radar can be created with the required angular resolution ($\sim$1°) based on the scalable Horus design. Such a system would likely have $\sim$10,000 radiating elements. Since the total transmit power scales with the array size, the sensitivity of the system would rival that of the WSR-88D radar, but with all the advantages of the fully digital Horus weather radar. The outlook is bright for fully digital phased array radars and Horus stands as just one example of what is possible for the future of weather monitoring.

ACKNOWLEDGMENT

REFERENCES

[1] I. M. Goklany, "Deaths and death rates from extreme weather events: 1900–2008," *J. Amer. Phys. Surg.*, vol. 13, pp. 102–109, Jan. 2009.

[2] D. S. Zrnic et al., "Agile-beam phased array radar for weather observations," *Bull. Amer. Meteorolog. Soc.*, vol. 88, no. 11, pp. 1753–1766, Nov. 2007, doi: 10.1175/BAMS-88-11-1753.

[3] H. B. Bluestein, M. M. French, I. PopStefanija, R. T. Bluth, and J. B. Knorr, "A mobile, phased-array Doppler radar for the study of severe convective storms: THE MWR-05XP," *Bull. Amer. Meteorolog. Soc.*, vol. 91, no. 5, pp. 579–600, May 2010, doi: 10.1175/2009BAMS2914.1.

[4] P. Kollias, D. J. McLaughlin, S. Frasier, M. Oue, E. Luke, and A. Sneddon, "Advances and applications in low-power phased array X-band weather radars," in *Proc. IEEE Radar Conf.*, Apr. 2018, pp. 1359–1364, doi: 10.1109/RADAR.2018.8378762.

[5] F. Mizutani et al., "Fast-scanning phased-array weather radar with angular imaging technique," *IEEE Trans. Geosci. Remote Sens.*, vol. 56, no. 5, pp. 2664–2673, May 2018, doi: 10.1109/TGRS.2017.2780847.

[6] M. Weber et al., "Towards the next generation operational meteorological radar," *Bull. Amer. Meteorolog. Soc.*, vol. 102, no. 7, pp. E1357–E1383, Jul. 2021, doi: 10.1175/BAMS-D-20-0067.1.

[7] R. Palmer et al., "A primer on phased array radar technology for the atmospheric sciences," *Bull. Amer. Meteorolog. Soc.*, vol. 103, no. 10, pp. E2391–E2416, Oct. 2022, doi: 10.1175/BAMS-D-21-0172.1.

[8] J. E. Stailey and K. D. Hondl, "Multifunction phased array radar for aircraft and weather surveillance," *Proc. IEEE*, vol. 104, no. 3, pp. 649–659, Mar. 2016, doi: 10.1109/JPROC.2015.2491179.

[9] P. L. Heinselman, D. L. Priegnitz, K. L. Manross, T. M. Smith, and R. W. Adams, "Rapid sampling of severe storms by the national weather radar testbed phased array radar," *Weather Forecasting*, vol. 23, no. 5, pp. 808–824, Oct. 2008, doi: 10.1175/2008WAF2007071.1.

[10] P. Kollias et al., "Science applications of phased array radars," *Bull. Amer. Meteorological Soc.*, vol. 103, no. 10, pp. E2370–E2390, 2022.

[11] H. Kikuchi et al., "Initial observations for precipitation cores with X-band dual polarized phased array weather radar," *IEEE Trans. Geosci. Remote Sens.*, vol. 58, no. 5, pp. 3657–3666, May 2020, doi: 10.1109/TGRS.2019.2959628.

[12] T. Ushio et al., "Recent progress on the phased array weather radar at X band," in *Proc. IEEE Radar Conf.*, Mar. 2022, pp. 1–4, doi: 10.1109/RADARCONF2248738.2022.9764164.

[13] C. Wu, L. Liu, X. Liu, G. Li, and C. Chen, "Advances in Chinese dual-polarization and phased-array weather radars: Observational analysis of a supercell in Southern China," *J. Atmos. Ocean. Technol.*, vol. 35, no. 9, pp. 1785–1806, Sep. 2018, doi: 10.1175/JTECH-D-17-0078.1.

[14] Z. Yu, B. Lan-Qiang, M. Zhi-Yong, C. Bing-Hong, T. Cong-Cong, and F. Pei-Ling, "Rapid-scan and polarimetric phased-array radar observations of a Tornado in the pearl river estuary," *J. Tropical Meteorol.*, vol. 26, no. 3, pp. 81–86, 2020.

[15] T.-Y. Yu, M. S. McCord, J. L. Salazar, C. Fulton, R. D. Palmer, and H. Bluestein, "Development of a shared mobile C-band polarimetric atmospheric imaging radar (PAIR)," in *Proc. Amer. Me Soc. 39th Conf. Radar Meteorol.*, Sep. 2019, pp. 1–16.

[16] I. Ivic et al., "An overview of weather calibration for the advanced technology demonstrator," in *Proc. IEEE Int. Symp. Phased Array Syst. Technol. (PAST)*, Oct. 2019, pp. 1–13.

[17] I. R. Ivić and D. Schvartzman, "Weather calibration efforts on the advanced technology demonstrator," in *Proc. 100rd Amer. Meteorolog. Soc. Annu. Meeting*, 2020, pp. 1–15.

[18] G. Zhang, R. J. Doviak, D. S. Zrnić, R. Palmer, L. Lei, and Y. Al-Rashid, "Polarimetric phased-array radar for weather measurement: A planar or cylindrical configuration?" *J. Atmos. Ocean. Technol.*, vol. 28, no. 1, pp. 63–73, Jan. 2011.

[19] C. Fulton et al., "Cylindrical polarimetric phased array radar: Beamforming and calibration for weather applications," *IEEE Trans. Geosci. Remote Sens.*, vol. 55, no. 5, pp. 2827–2841, May 2017.

[20] J. S. Herd and M. D. Conway, "The evolution to modern phased array architectures," *Proc. IEEE*, vol. 104, no. 3, pp. 519–529, Mar. 2016.

[21] C. Fulton, M. Yeary, D. Thompson, J. Lake, and A. Mitchell, "Digital phased arrays: Challenges and opportunities," *Proc. IEEE*, vol. 104, no. 3, pp. 487–503, Mar. 2016, doi: 10.1109/JPROC.2015.2501804.

[22] R. D. Palmer, C. J. Fulton, J. Salazar, H. Sigmarsson, and M. Yeary, "The 'Horus' radar—An all-digital polarimetric phased array radar for multi-mission surveillance," in *Proc. 99th Amer. Meteorolog. Soc. Annu. Meeting*, Phoenix, AZ, USA, 2019, pp. 1–20.

[23] R. D. Palmer et al., "Horus—An all-digital phased array weather radar developed at the university of Oklahoma," in *Proc. 103rd AMS Annu. Meeting*, 2023, pp. 1–22.

[24] T. D. Crum and R. L. Alberty, "The WSR-88D and the WSR-88D operational support facility," *Bull. Amer. Meteorol. Soc.*, vol. 74, no. 9, pp. 1669–1688, 1993.

[25] R. J. Doviak and D. Zrnic, *Doppler Radar and Weather Observations*. New York, NY, USA: Dover, 2006.

[26] M. M. French, H. B. Bluestein, I. PopStefanija, C. A. Baldi, and R. T. Bluth, "Reexamining the vertical development of tornadic vortex signatures in supercells," *Monthly Weather Rev.*, vol. 141, no. 12, pp. 4576–4601, Dec. 2013.

[27] J. B. Houser, H. B. Bluestein, and J. C. Snyder, "Rapid-scan, polarimetric, Doppler radar observations of tornadogenesis and Tornado dissipation in a tornadic supercell: The 'El Reno, Oklahoma' storm of 24 May 2011," *Monthly Weather Rev.*, vol. 143, no. 7, pp. 2685–2710, 2015.

[28] D. J. Bodine et al., "Observations of severe local storms and tornadoes with the atmospheric imaging radar," *Bull. Amer. Meteorolog. Soc.*, vol. 98, no. 5, pp. 915–935, May 2017, doi: 10.1175/BAMS-D-15-00266.1.

[29] S. M. Torres et al., "Adaptive-weather-surveillance and multifunction capabilities of the national weather radar testbed phased array radar," *Proc. IEEE*, vol. 104, no. 3, pp. 660–672, Mar. 2016, doi: 10.1109/JPROC.2015.2484288.

[30] D. Schvartzman, "Signal processing techniques and concept of operations for polarimetric rotating phased array radar," Ph.D. dissertation, School Elect. Comput. Eng., The Univ. Oklahoma, Norman, OK, USA, 2020.

[31] D. Schvartzman, S. M. Torres, and T. Yu, "Integration of the motion-compensated steering and distributed beams' techniques for polarimetric rotating phased array radar," IEEE Geosci. Remote Sens. Lett., vol. 19, pp. 1–5, 2022, doi: 10.1109/LGRS.2021.3113564.

[32] B. Isom et al., "The atmospheric imaging radar: Simultaneous volumetric observations using a phased array weather radar," J. Atmos. Ocean. Technol., vol. 30, no. 4, pp. 655–675, Apr. 2013, doi: 10.1175/JTECH-D-12-00063.1.

[33] D. Schvartzman, S. M. Torres, and T. Yu, "Distributed beams: Concept of operations for polarimetric rotating phased array radar," IEEE Trans. Geosci. Remote Sens., vol. 59, no. 11, pp. 9173–9191, Nov. 2021, doi: 10.1109/TGRS.2020.3047090.

[34] G. Buttazzoni and R. Vescovo, "An efficient and versatile technique for the synthesis of 3D copolar and crosspolar patterns of phase-only reconfigurable conformal arrays with DRR and near-field control," IEEE Trans. Antennas Propag., vol. 62, no. 4, pp. 1640–1651, Apr. 2014, doi: 10.1109/TAP.2014.2308319.

[35] D. P. Scholnik, "A parameterized pattern-error objective for large-scale phase-only array pattern design," IEEE Trans. Antennas Propag., vol. 64, no. 1, pp. 89–98, Jan. 2016, doi: 10.1109/TAP.2015.2500239.

[36] D. Schvartzman, J. D. D. Díaz, J. L. Salazar-Cerreño, T. Yu, R. D. Palmer, and M. S. McCord, "A hybrid antenna pattern synthesis method for the polarimetric atmospheric imaging radar (PAIR)," in Proc. IEEE Radar Conf., Mar. 2022, pp. 1–6, doi: 10.1109/Radar-Conf2248738.2022.9764359.

[37] R. J. Reinke, D. Schvartzman, F. Nai, T. Yu, J. Salazar-Cerreño, and R. D. Palmer, "Evaluation of a spline-based parameterization scheme for phase-only antenna pattern synthesis," in Proc. IEEE Int. Symp. Phased Array Syst. Technol. (PAST), Oct. 2022, pp. 1–8, doi: 10.1109/PAST49659.2022.9975004.

[38] D. S. Zrnic, V. M. Melnikov, R. J. Doviak, and R. Palmer, "Scanning strategy for the multifunction phased-array radar to satisfy aviation and meteorological needs," IEEE Geosci. Remote Sens. Lett., vol. 12, no. 6, pp. 1204–1208, Jun. 2015, doi: 10.1109/LGRS.2014.2388202.

[39] D. Schvartzman, M. Weber, S. Torres, H. Thomas, D. S. Zrnic, and I. Ivic, "Scanning concepts and architectures supporting rotating meteorological phased-array radar," in Proc. 101st Amer. Meteorolog, Soc. Annu. Meeting, 2021, pp. 1–10.

[40] J. Capon, "High-resolution frequency-wavenumber spectrum analysis," Proc. IEEE, vol. 57, no. 8, pp. 1408–1418, Jan. 1969.

[41] P. Stoica and R. Moses, Spectral Analysis of Signals. London, U.K.: Pearson, 2005.

[42] B. M. Isom et al., "A new frontier for mobile radar—The atmospheric imaging radar: Design specifications and experimental functionality," in Proc. 34th Conf. Radar Meteorol., A. M. Soc. Ed., Williamsburg, VA, USA, 2009, pp. 1–22.

[43] L. Norin, "A quantitative analysis of the impact of wind turbines on operational Doppler weather radar data," Atmos. Meas. Techn., vol. 8, no. 2, pp. 593–609, Feb. 2015, doi: 10.5194/amt-8-593-2015.

[44] F. Uysal, I. Selesnick, and B. M. Isom, "Mitigation of wind turbine clutter for weather radar by signal separation," IEEE Trans. Geosci. Remote Sens., vol. 54, no. 5, pp. 2925–2934, May 2016, doi: 10.1109/TGRS.2015.2508380.

[45] D. Schvartzman, "Mitigation of wind turbine clutter with digital phased array radar," IEEE Access, vol. 11, pp. 12911–12924, 2023.

[46] W. L. Melvin, "A STAP overview," IEEE Aerosp. Electron. Syst. Mag., vol. 19, no. 1, pp. 19–35, Jan. 2004, doi: 10.1109/MAES.2004.1263229.

[47] B. Luijten et al., "Adaptive ultrasound beamforming using deep learning," IEEE Trans. Med. Imag., vol. 39, no. 12, pp. 3967–3978, Dec. 2020, doi: 10.1109/TMI.2020.3008537.

[48] T. Lin and Y. Zhu, "Beamforming design for large-scale antenna arrays using deep learning," IEEE Wireless Commun. Lett., vol. 9, no. 1, pp. 103–107, Jan. 2020, doi: 10.1109/LWC.2019.2943466.

[49] H. Kikuchi, E. Yoshikawa, T. Ushio, and Y. Hobara, "Clutter reduction for phased-array weather radar using diagonal capon beamforming with neural networks," IEEE Geosci. Remote Sens. Lett., vol. 17, no. 12, pp. 2065–2069, Dec. 2020, doi: 10.1109/LGRS.2019.2962558.

[50] Y. Kim, D. Schvartzman, R. D. Palmer, and T. Yu, "Fast adaptive beamforming using deep learning for digital phased array radars," in Proc. IEEE Int. Symp. Phased Array Syst. Technol. (PAST), Oct. 2022, pp. 1–7, doi: 10.1109/PAST49659.2022.9975038.

[51] Z. Li, T. Cheng, and S. Heng, "Real-time dwell scheduling algorithm for phased array radar based on a backtracking strategy," IET Radar, Sonar Navigat., vol. 17, no. 2, pp. 261–276, Feb. 2023, doi: 10.1049/rsn2.12339.

[52] M. L. Manna, P. Monsurrò, P. Tommasino, and A. Trifiletti, "Machine learning techniques for frequency sharing in a cognitive radar," in Proc. IEEE Radar Conf., Apr. 2018, pp. 732–735, doi: 10.1109/RADAR.2018.8378650.

[53] M. S. Veillette, J. M. Kurdzo, P. M. Stepanian, J. McDonald, S. Samsi, and J. Y. N. Cho, "A deep learning-based velocity dealiasing algorithm derived from the WSR-88D open radar product generator," 2022, arXiv:2211.13181.

[54] D. S. Zrnic and A. V. Ryzhkov, "Polarimetry for weather surveillance radars," Bull. Amer. Meteorolog. Soc., vol. 80, no. 3, pp. 389–406, Mar. 1999.

[55] A. V. Ryzhkov, T. J. Schuur, D. W. Burgess, P. L. Heinselman, S. E. Giangrande, and D. S. Zrnic, "The joint polarization experiment: Polarimetric rainfall measurements and hydrometeor classification," Bull. Amer. Meteorolog. Soc., vol. 86, no. 6, pp. 809–824, Jun. 2005, doi: 10.1175/BAMS-86-6-809.

[56] A. Ryzhkov, M. Diederich, P. Zhang, and C. Simmer, "Potential utilization of specific attenuation for rainfall estimation, mitigation of partial beam blockage, and radar networking," J. Atmos. Ocean. Technol., vol. 31, no. 3, pp. 599–619, Mar. 2014, doi: 10.1175/JTECH-D-13-00038.1.

[57] R. L. Ice et al., "Monitoring the performance of the polarimetric WSR-88D—Calibration and sensitivity," in Proc. 33rd Conf. Environ. Inf. Process. Technol., 2017, pp. 1–14.

[58] I. Ivić and D. Schvartzman, "A first look at the ATD data corrections. preprints," in Proc. 39th Int. Conf. Radar Meteorol., 2019, pp. 2–6.

[59] C. Fulton et al., "Mutual coupling-based calibration for the Horus digital phased array radar," in Proc. IEEE Int. Symp. Phased Array Syst. Technol. (PAST), Oct. 2022, pp. 1–6.

[60] D. Zrnić, R. Doviak, G. Zhang, and A. Ryzhkov, "Bias in differential reflectivity due to cross coupling through the radiation patterns of polarimetric weather radars," J. Atmos. Ocean. Technol., vol. 27, no. 10, pp. 1624–1637, Oct. 2010, doi: 10.1175/2010JTECHA1350.1.

[61] M. Sánchez-Barbetty, R. W. Jackson, and S. Frasier, "Interleaved sparse arrays for polarization control of electronically steered phased arrays for meteorological applications," IEEE Trans. Geosci. Remote Sens., vol. 50, no. 4, pp. 1283–1290, Apr. 2012, doi: 10.1109/TGRS.2011.2167016.

[62] M. Yeary, D. Conway, J. Herd, M. Fosberry, M. Harger, and K. Hondl, "A method for improved cross-pol isolation based on the use of auxilliary elements," in Proc. IEEE Int. Symp. Phased Array Syst. Technol., Oct. 2013, pp. 272–275, doi: 10.1109/ARRAY.2013.6731840.

[63] C. Salazar, D. Schvartzman, B. Cheong, and R. D. Palmer, "Cross-polar canceller (XPC): A technique to reduce Cross-polar pattern contamination in polarimetric weather observations," in Proc. IEEE Int. Symp. Phased Array Syst. Technol. (PAST), Oct. 2022, pp. 1–8, doi: 10.1109/PAST49659.2022.9975050.

[64] W. M. Jones and P. Delos, "Novel all-digital beamforming techniques for L/S/C-band multi-channel systems leveraging hardened DSP on integrated circuits," in Proc. IEEE Int. Symp. Phased Array Syst. Technol. (PAST), Oct. 2022, pp. 1–8.

[65] J. D. Diaz, "Ultra-low cross polarization antenna architectures for multi-function planar phased arrays," Ph.D. dissertation, School Elect. Comput. Eng., Univ. Oklahoma, Norman, OK, USA, 2021.

[66] B. James and C. Fulton, "Decorrelation and mitigation of spurious products in phased arrays with direct conversion transceivers," in IEEE MTT-S Int. Microw. Symp. Dig., May 2015, pp. 1–4, doi: 10.1109/MWSYM.2015.7166990.

[67] N. Peccarelli, B. James, C. Fulton, and N. Goodman, "Dynamic range considerations for modern digital array radars," in Proc. IEEE Int. Radar Conf. (RADAR), Apr. 2020, pp. 578–583, doi: 10.1109/RADAR42522.2020.9114607.

[68] P. Delos, "A review of wideband RF receiver architecture options," Analog Devices, Wilmington, MA, USA, Tech. Rep., 2017, pp. 1–3. [Online]. Available: https://www.analog.com/en/technical-articles/a-review-of-wideband-rf-receiver-architecture-options.html

[69] B. Brannon, "Where zero-IF wins: 50% smaller PCB footprint at 1/3 the cost," Analog Dialogue, vol. 50, pp. 1–7, Sep. 2016.

[70] M. Skolnik, Radar Handbook, 3rd ed. New York, NY, USA: McGraw-Hill, 2008.

[71] O. Somerlock et al., "An X-band element-level digital receive array," in Proc. IEEE Int. Symp. Phased Array Syst. Technol. (PAST), Oct. 2016, pp. 1–8.

[72] R. Doviak, D. Zrnić, and D. Sirmans, "Doppler weather radar," *Proc. IEEE*, vol. 67, no. 11, pp. 1522–1553, Nov. 1979.

[73] G. Ariturk, N. R. Almuqati, and H. H. Sigmarsson, "Element-level microwave filter integration in fully-digital phased array radar systems," in *Proc. IEEE 22nd Annu. Wireless Microw. Technol. Conf.*, Apr. 2022, pp. 1–4.

[74] R. Irazoqui, "An investigation and solution to spatial interferers before RF front end for phased arrays," Ph.D. dissertation, School Elect. Comput. Eng., Univ. Oklahoma, Norman, OK, USA, 2019.

[75] M. J. Hainz, S. Mischorr, and P. E. Pace, "FPGA compression process for number theoretic CW radar with increased unambiguous detection range," in *Proc. IEEE Radar Conf. (RadarConf)*, Apr. 2019, pp. 1–6.

[76] B. Schweizer et al., "The fairy tale of simple all-digital radars: How to deal with 100 Gbit/s of a digital millimeter-wave MIMO radar on an FPGA," *IEEE Microw. Mag.*, vol. 22, no. 7, pp. 66–76, Jul. 2021.

[77] J. D. Díaz et al., "A cross-stacked radiating antenna with enhanced scanning performance for digital beamforming multifunction phased-array radars," *IEEE Trans. Antennas Propag.*, vol. 66, no. 10, pp. 5258–5267, Oct. 2018.

[78] M. Herndon, M. Yeary, and R. Palmer, "Studies of front-end distortion characterization via mutual coupling measurements in phased array systems," in *Proc. IEEE Int. Radar Conf. (RADAR)*, Apr. 2020, pp. 798–803.

[79] S. H. Talisa, K. W. O'Haver, T. M. Comberiate, M. D. Sharp, and O. F. Somerlock, "Benefits of digital phased array radars," *Proc. IEEE*, vol. 104, no. 3, pp. 530–543, Mar. 2016, doi: 10.1109/JPROC.2016.2515842.

[80] W. T. Patton and L. H. Yorinks, "Near-field alignment of phased-array antennas," *IEEE Trans. Antennas Propag.*, vol. 47, no. 3, pp. 584–591, Mar. 1999.

[81] B. Harker, "Dynamic range improvements and measurements in radar systems," *IET Radar, Sonar Navigat.*, vol. 1, no. 8, pp. 398–406, Dec. 2007.

[82] N. Peccarelli, R. Irazoqui, and C. Fulton, "Mitigation of interferers and nonlinear spurious products for digital array and MIMO systems," in *IEEE MTT-S Int. Microw. Symp. Dig.*, Jun. 2019, pp. 1233–1236, doi: 10.1109/MWSYM.2019.8701111.

[83] N. Peccarelli and C. Fulton, "A mutual coupling approach to digital pre-distortion and nonlinear equalization calibration for digital arrays," in *Proc. IEEE Int. Symp. Phased Array Syst. Technol. (PAST)*, Oct. 2019, pp. 1–8.

[84] C. A. Balanis, *Antenna Theory: Analysis and Design*. Hoboken, NJ, USA: Wiley, 2005.

[85] G. Zhang, R. J. Doviak, D. S. Zrnic, J. Crain, D. Staiman, and Y. Al-Rashid, "Phased array radar polarimetry for weather sensing: A theoretical formulation for bias corrections," *IEEE Trans. Geosci. Remote Sens.*, vol. 47, no. 11, pp. 3679–3689, Nov. 2009.

[86] S. Duthoit et al., "A new approach for in-situ antenna characterization, radome inspection and radar calibration, using an unmanned aircraft system (UAS)," in *Proc. IEEE Radar Conf. (RadarConf)*, May 2017, pp. 669–674.

[87] M. García-Fernández et al., "Antenna diagnostics and characterization using unmanned aerial vehicles," *IEEE Access*, vol. 5, pp. 23563–23575, 2017, doi: 10.1109/ACCESS.2017.2754985.

[88] J. L. Salazar, A. Umeyama, S. Duthoit, and C. Fulton, "UAS-based antenna pattern measurements and radar characterization," in *Proc. IEEE Conf. Antenna Meas. Appl. (CAMA)*, Sep. 2018, pp. 1–4.

[89] C. Culotta-López et al., "On the uncertainty sources of drone-based outdoor far-field antenna measurements," in *Proc. Antenna Meas. Techn. Assoc. Symp. (AMTA)*, Oct. 2021, pp. 1–6, doi: 10.23919/AMTA52830.2021.9620638.

[90] A. Segales et al., "Development of a technique for scanning antenna patterns using unmanned aircraft systems," presented at the 103rd AMS Annu. Meeting, 2023.

[91] C. Wasserzier, J. G. Worms, and D. W. O'Hagan, "A concept for far field measurements of large dimension antennas in an open area test site performed by UAS," in *Proc. 20th Int. Radar Symp. (IRS)*, Jun. 2019, pp. 1–10, doi: 10.23919/IRS.2019.8768157.

[92] A. Y. Umeyama, J. L. Salazar-Cerreno, and C. Fulton, "UAV-based antenna measurements for polarimetric weather radars: Probe analysis," *IEEE Access*, vol. 8, pp. 191862–191874, 2020, doi: 10.1109/ACCESS.2020.3027779.

[93] A. Y. Umeyama, J. L. Salazar-Cerreno, and C. J. Fulton, "UAV-based far-field antenna pattern measurement method for polarimetric weather radars: Simulation and error analysis," *IEEE Access*, vol. 8, pp. 191124–191137, 2020, doi: 10.1109/ACCESS.2020.3027790.

[94] T. B. Hansen and A. D. Yaghjian, *Plane-Wave Theory of Time-Domain Fields: Near-Field Scanning Applications*. Piscataway, NJ, USA: Wiley, 1999.

[95] D. J. van Rensburg, "Limitations of near-field back projection for phased array tuning applications," in *Proc. AMTA*, 2001. [Online]. Available: https://www.nsi-mi.com/images/Technical_Papers/2001/01DjVR-Limitations-of-NF-back-projection.pdf

[96] C. Fulton et al., "Mutual coupling-based calibration for the Horus digital phased array radar," in *Proc. IEEE Int. Symp. Phased Array Syst. Technol. (PAST)*, Oct. 2022, pp. 1–6, doi: 10.1109/PAST49659.2022.9974962.

[97] D. Schvartzman et al., "A polarimetric antenna-calibration method for the Horus radar based on E-field back projection," in *Proc. IEEE Int. Symp. Phased Array Syst. Technol. (PAST)*, Oct. 2022, pp. 1–7, doi: 10.1109/PAST49659.2022.9975030.

[98] J. T. Logan, D. S. Reinhard, and K. E. Hauck, "Phased array calibration and diagnostics utilizing a student-built planar near-field system," in *Proc. IEEE Int. Symp. Phased Array Syst. Technol.*, Oct. 2010, pp. 279–286, doi: 10.1109/ARRAY.2010.5613358.

[99] I. R. Ivic and R. J. Doviak, "Evaluation of phase coding to mitigate differential reflectivity bias in polarimetric PAR," *IEEE Trans. Geosci. Remote Sens.*, vol. 54, no. 1, pp. 431–451, Jan. 2016, doi: 10.1109/TGRS.2015.2459047.

[100] I. R. Ivić, "An approach to simulate the effects of antenna patterns on polarimetric variable estimates," *J. Atmos. Ocean. Technol.*, vol. 34, no. 9, pp. 1907–1934, Sep. 2017, doi: 10.1175/JTECH-D-17-0015.1.

[101] D. Zrnic, D. Schvartzman, J. D. D. Díaz, R. D. Palmer, and A. Ryzhkov, "Effects of Horus antenna patterns on polarimetric weather observations," in *Proc. IEEE Int. Symp. Phased Array Syst. Technol. (PAST)*, Oct. 2022, pp. 1–7, doi: 10.1109/PAST49659.2022.9975016.

[102] H. M. Aumann, A. J. Fenn, and F. G. Willwerth, "Phased array antenna calibration and pattern prediction using mutual coupling measurements," *IEEE Trans. Antennas Propag.*, vol. 37, no. 7, pp. 844–850, Jul. 1989.

[103] D. Bekers, R. van Dijk, and F. van Vliet, "Mutual-coupling based phased-array calibration: A robust and versatile approach," in *Proc. IEEE Int. Symp. Phased Array Syst. Technol.*, Oct. 2013, pp. 630–637, doi: 10.1109/ARRAY.2013.6731903.

[104] S. M. Torres, C. D. Curtis, and D. Schvartzman, "Requirement-driven design of pulse compression waveforms for weather radars," *J. Atmos. Ocean. Technol.*, vol. 34, no. 6, pp. 1351–1369, Jun. 2017, doi: 10.1175/JTECH-D-16-0231.1.

[105] C. M. Salazar Aquino, B. Cheong, and R. D. Palmer, "Progressive pulse compression: A novel technique for blind range recovery for solid-state radars," *J. Atmos. Ocean. Technol.*, pp. 1599–1611, Jul. 2021, doi: 10.1175/JTECH-D-20-0164.1.

[106] C. M. Salazar Aquino, B. Cheong, R. D. Palmer, D. Schvartzman, and A. Ryzhkov, "Salient improvements in the progressive pulse compression technique," *J. Atmos. Ocean. Technol.*, submitted for publication.

[107] P. H. Hildebrand and R. S. Sekhon, "Objective determination of the noise level in Doppler spectra," *J. Appl. Meteorol.*, vol. 13, no. 7, pp. 808–811, Oct. 1974.

[108] J. Y. N. Cho, "A new radio frequency interference filter for weather radars," *J. Atmos. Ocean. Technol.*, vol. 34, no. 7, pp. 1393–1406, Jul. 2017, doi: 10.1175/JTECH-D-17-0028.1.

[109] A. Siggia and R. Passarelli, "Gaussian model adaptive processing (GMAP) for improved ground clutter cancellation and moment calculation," in *Proc. ERAD*, vol. 2, 2004, pp. 421–424.

[110] L. Lei et al., "Multilag correlation estimators for polarimetric radar measurements in the presence of noise," *J. Atmos. Ocean. Technol.*, vol. 29, no. 6, pp. 772–795, Jun. 2012, doi: 10.1175/JTECH-D-11-00010.1.

[111] D. Warde, D. Schvartzman, and C. D. Curtis, "Generalized multilag estimators (GMLE) for polarimetric weather radar observations," *IEEE Trans. Geosci. Remote Sens.*, early access, May 22, 2023, doi: 10.1109/TGRS.2023.3278489.

[112] J. R. Adam, N. R. Lindblad, and C. D. Hendricks, "The collision, coalescence, and disruption of water droplets," *J. Appl. Phys.*, vol. 39, no. 11, pp. 5173–5180, Oct. 1968, doi: 10.1063/1.1655940.

[113] A. Ryzhkov and D. Zrnic, *Radar Polarimetry for Weather Observations* (Springer Atmospheric Sciences). Cham, Switzerland: Springer, 2019.

[114] I. R. Ivić, "On the use of a radial-based noise power estimation technique to improve estimates of the correlation coefficient on dual-polarization weather radars," *J. Atmos. Ocean. Technol.*, vol. 31, no. 9, pp. 1867–1880, Sep. 2014, doi: 10.1175/JTECH-D-14-00052.1.

[115] A. Ryzhkov and J. Krause, "New polarimetric radar algorithm for melting layer detection and determination of its height," *J. Atmos. Ocean. Technol.*, vol. 39, pp. 529–543, May 2022, doi: doi:.10.1175/JTECH-D-21-0130.1.

[116] K. L. Ortega, J. M. Krause, and A. V. Ryzhkov, "Polarimetric radar characteristics of melting Hail. Part III: Validation of the algorithm for hail size discrimination," *J. Appl. Meteorol. Climatol.*, vol. 55, no. 4, pp. 829–848, Apr. 2016, doi: 10.1175/JAMC-D-15-0203.1.

[117] V. M. Melnikov and D. Zrnic, "Simultaneous transmission mode for the polarimetric WSR-88D: Statistical biases and standard deviations of polarimetric variables," Cooperat. Inst. Mesoscale Meteorol. Stud., Univ. Oklahoma, Norman, OK, USA, Tech. Rep., 2004. [Online]. Available: https://www.nssl.noaa.gov/publications/wsr88d_reports/SHV_statistics.pdf

[118] *Radar Functional Requirement*, NOAA/NWS, Washington, DC, USA, 2015. [Online]. Available: https://www.roc.noaa.gov/WSR88D/PublicDocs/NOAA_Radar_Functional_Requirements_Final_Sept%202015.pdf

[119] A. D. Byrd, R. D. Palmer, and C. J. Fulton, "Development of a low-cost multistatic passive weather radar network," *IEEE Trans. Geosci. Remote Sens.*, vol. 58, no. 4, pp. 2796–2808, Apr. 2020, doi: 10.1109/TGRS.2019.2955606.

[120] A. D. Byrd, R. D. Palmer, and C. J. Fulton, "Doppler velocity bias mitigation through sidelobe whitening for multistatic weather radar," *IEEE Trans. Geosci. Remote Sens.*, vol. 59, no. 2, pp. 1130–1142, Feb. 2021, doi: 10.1109/TGRS.2020.2997882.

David Schvartzman (Senior Member, IEEE) was born in Piracicaba, Brazil, in March 1988. He received the B.S. degree in electrical and computer engineering from the National University of Asunción, San Lorenzo, Paraguay, in 2011, and the M.S. and Ph.D. degrees in electrical and computer engineering from The University of Oklahoma (OU), Norman, OK, USA, in 2015 and 2020, respectively.

From 2015 to 2020, he was a Research Scientist with the NOAA National Severe Storms Laboratory (NSSL) and the Cooperative Institute for Severe and High-Impact Weather Research and Operations (CIWRO). From 2021 to 2022, he was a Research Scientist with the Advanced Radar Research Center (ARRC), OU. He is currently an Assistant Professor with the School of Meteorology, OU, affiliated with the ARRC. He is also an Adjunct Assistant Professor with the School of Electrical and Computer Engineering, OU. He works on novel signal and array processing algorithms to improve the understanding of atmospheric processes using phased array radar. He also works on the calibration and integration of phased-array radar systems. He is a member of the American Meteorological Society (AMS). He was a recipient of the 2019 American Meteorological Society's Spiros G. Geotis Prize.

Robert D. Palmer (Fellow, IEEE) was born in Fort Benning, GA, USA, on June 1962. He received the Ph.D. degree in electrical engineering from The University of Oklahoma (OU), Norman, OK, USA, in 1989.

From 1989 to 1991, he was a JSPS Post-Doctoral Fellow with the Radio Atmospheric Science Center, Kyoto University, Japan, where his major accomplishment was the development of novel interferometric radar techniques for studies of atmospheric turbulent layers. After his stay in Japan, he was with the Department of Physics and Astronomy, Clemson University, South Carolina. From 1993 to 2004, he was a part of the faculty of the Department of Electrical Engineering, University of Nebraska–Lincoln, where his interests broadened into areas including wireless communications, remote sensing, and pedagogy. Soon after moving to OU as the Tommy C. Craighead Chair at the School of Meteorology in 2004, he established the interdisciplinary Advanced Radar Research Center (ARRC). He currently serves as the Executive Director for the ARRC and OU's Associate Vice President for Research and Partnerships. While at OU, his research interests have focused on the application of advanced radar signal processing techniques to observations of severe weather, particularly related to phased-array radars and other innovative system designs. He has published widely in the area of radar sensing of the atmosphere, with over 115 peer-reviewed journal articles, one textbook, 40 international invited talks, and more than 300 conference presentations.

Prof. Palmer is a fellow of the American Meteorological Society (AMS) emphasizing his dedication to the interdisciplinary nature of radar science.
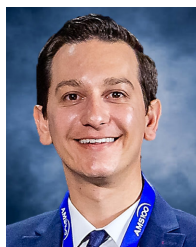
Mark B. Yeary (Fellow, IEEE) received the Ph.D. degree from the Department of Electrical Engineering, Texas A&M University, College Station, TX, USA, in 1999.

Since the Fall 2002, he has been with the School of Electrical and Computer Engineering, The University of Oklahoma (OU), Norman, OK, USA, where he was named the endowed Hudson-Torchmark Presidential Professor in 2011. As of 2005, he is also a Founding Member of the Advanced Radar Research Center (ARRC), OU, which is now the largest university-based radar center in the nation. For instance, he was deeply involved in the National Weather Radar Testbed, the ARRC's Atmospheric Imaging Radar Program, and the ARRC's Horus Program. He has served as a PI or Co-PI on grants from ONR, NASA, NSF, NOAA, and DARPA. His research interests include digital signal processing and radar systems with an emphasis on hardware prototype development.

Dr. Yeary is a fellow of the Cooperative Institute for Severe and High-Impact Weather Research and Operations (CIWRO), National Weather Center, Norman. In 2022, he was awarded OU's George Lynn Cross Research Professorship and named the Gallogy Chair Professorship within OU's Gallogly College of Engineering. He serves as a Faculty Advisor to OU's American Indians in Science and Engineering Society (AISES) Chapter. He served as the Co-Chair for the 2018 IEEE Radar Conference. Since 2009, he has been the Chair of the radar sessions at the American Meteorological Society (AMS) Annual Meetings. He is a licensed Professional Engineer.

Jorge L. Salazar-Cerreno (Senior Member, IEEE) received the B.S. degree in electronics and communications engineering from University Antenor Orrego, Trujillo, Peru, the M.S. degree in electronics and communications engineering from the University of Puerto Rico, Mayagüez (UPRM), in 2011, and the Ph.D. degree in electronics and communications engineering from the University of Massachusetts, Amherst. His Ph.D. research focused on the development of low-cost dual-polarized active phased array antennas (APAA). After graduation, he was awarded a prestigious National Center for Atmospheric Research (NCAR) Advanced Study Program (ASP) Post-Doctoral Fellowship. He joined the Advanced Radar Research Center (ARRC), The University of Oklahoma, as a Research Scientist, and became an Assistant Professor with the School of Electrical and Computer Engineering in August 2015. He has recently been promoted to the rank of Associate Professor. His research interests include high-performance, broadband antennas for dual-polarized phased array radar applications, array antenna architecture for reconfigurable radar systems, APAA, Tx/Rx modules, radome EM modeling, and millimeter-wave antennas. In 2019, he was awarded the prestigious William H. Barkow Presidential Professorship from The University of Oklahoma for meeting the highest standards of excellence in scholarship and teaching. He is a reviewer of various IEEE and AMS conferences and journals.

Caleb Fulton (Senior Member, IEEE) received the B.S. and Ph.D. degrees in electrical and computer engineering from Purdue University, West Lafayette, IN, USA, in 2006 and 2011, respectively, where he lead the development of the Army Digital Array Radar Demonstrator.

He is currently an Associate Professor in electrical and computer engineering with the Advanced Radar Research Center, The University of Oklahoma, Norman, OK, USA, where he is involved in a number of digital phased array research and development efforts for a variety of applications. His research interests include antenna design and electromagnetic analysis, digital phased array calibration and compensation for transceiver errors, calibration for high-quality polarimetric radar measurements, integration of low-complexity transceivers and high-power GaN devices, and advanced digital beamforming design considerations.

Dr. Fulton is a member of the IEEE Antennas and Propagation Society, the IEEE Aerospace and Electronic Systems Society, and the IEEE Microwave Theory and Techniques Society. He serves on the Education Committee of the latter. He received the Purdue University Eaton Alumni Award for Design Excellence in 2009 for his work on the Army Digital Array Radar Project, the Meritorious Paper Award for a summary of these efforts at the 2010 Government Microcircuit Applications and Critical Technologies Conference, and the 2015 DARPA Young Faculty Award for his ongoing digital phased-array research.

Matthew McCord (Member, IEEE) received the B.S. degree in computer engineering and the M.S. degree in electrical and computer engineering from The University of Oklahoma (OU), Norman, OK, USA, in 2008 and 2012, respectively. From 2012 to 2014, he was with the Cooperative Institute for Mesoscale Meteorological Studies, OU, as a Research Associate affiliated with the National Severe Storms Laboratory (NSSL) supporting the National Weather Radar Testbed and KOUN, a WSR-88D research radar. In 2014, he joined the Advanced Radar Research Center, OU, where he is a Lead Radar Engineer. He specializes in developing advanced radar systems and hardware to resolve unique research challenges with an emphasis on phased arrays. While at the ARRC he has contributed to the development of the Cylindrical Polarimetric Phased Array Radar (CPPAR), the Polarimetric Atmospheric Imaging Radar (PAIR), and the fully digital Horus radar systems.

Boonleng Cheong received the Ph.D. degree in electrical engineering from the University of Nebraska–Lincoln, Lincoln, Nebraska, in 2005, with a dissertation titled "Adaptive Beamforming to Observe the Atmospheric Boundary Layer Using the Turbulent Eddy Profiler."

He joined The University of Oklahoma (OU) immediately after his graduation. From 2005 to 2007, he was a Post-Doctoral Fellow with the School of Meteorology. The opportunity allowed him to utilize his expertise in digital signal processing in the areas of remote sensing using ground-based radars. Since 2008, he has been with the Advanced Radar Research Center (ARRC), OU, as a Research Scientist. He is also with the School of Electrical and Computer Engineering (ECE), OU, as an Adjunct Associate Professor, and the Cooperative Institute for Severe and High-Impact Weather Research and Operations (CIWRO) as an Executive Board Member and Fellow. He has authored and coauthored more than 40 peer-reviewed journal articles and over 100 conference presentations and invited talks. Throughout his career, he has published in several internationally recognized scholarly journal magazines. His research interests include modern software-defined radar design, array signal processing, real-time software architecture, parallel computing, numerical simulations, and artificial intelligence using deep learning. He is the Key Developer of the PX-1000 and PX-10k systems, which are solid-state-based X-band polarimetric transportable radars.

David Bodine (Member, IEEE) received the B.S. and M.S. degrees in meteorology, the M.S. degree in electrical and computer engineering, and the Ph.D. degree in meteorology from The University of Oklahoma (OU), Norman, OK, USA, in 2007, 2009, 2012, and 2014, respectively.

His early research focused on boundary layer meteorology and understanding near-surface temperature and moisture variability. His Ph.D. research focused on dual-polarization radar signatures of supercells and tornadoes as well as numerical simulations of tornadoes and debris. After finishing his Ph.D. studies, he completed a Post-Doctoral Fellow with the National Center for Atmospheric Research (NCAR), analyzing mesoscale convective systems. In 2016, he joined the Advanced Radar Research Center (ARRC), OU, as a Research Scientist. In 2022, he became an Associate Professor with the School of Meteorology, OU. His primary research interests focus on understanding severe storms and other mesoscale phenomena using polarimetric and phased-array radar observations and high-resolution numerical simulations. In these research areas, he has published over 30 journal articles and 100 conference presentations.

Dr. David received the Outstanding Early Career Award from the American Meteorological Society's Scientific and Technological Activities Commission, in 2022. He serves on the American Meteorological Society (AMS) Committee on Radar Meteorology and is an Associate Editor for *Monthly Weather Review* and the *Journal of Applied Meteorology and Climatology*. He Co-Chaired the Phased Array Radar Symposium at the 99th AMS Annual Meeting. He is Co-Chairing the 2023 AMS Conference on Radar Meteorology.

Pierre Kirstetter (Senior Member, IEEE) received the M.Sc.Eng. degree from the Grenoble Institute of Technology, France, and the M.Sc. and Ph.D. degrees from Université Grenoble Alps, France. He was a CNES Post-Doctoral Fellow before working on NASA projects and a Research Scientist with the Advanced Radar Research Center, Norman, OK, USA. He is currently an Associate Professor with the School of Meteorology and the School of Civil Engineering and Environmental Science, The University of Oklahoma (OU), Norman, a Faculty Member with the Advanced Radar Research Center, and also affiliated with the National Severe Storms Laboratory, Norman. He investigates atmospheric precipitation and its impacts on climate, weather, hydrology, and society to address interdisciplinary and high-impact challenges spanning across agencies (e.g., NOAA and NASA) and communities (atmospheric sciences and hydrology). He led the development of the NOAA/OU multi-radar/multi-sensor system (MRMS) coincident data with NASA's Global Precipitation Measurement (GPM) mission sensors and their community use in satellite-based precipitation, with applications in numerical and weather prediction, natural disaster prediction, water resources, and study of the global water cycle. He has demonstrated the benefit of precipitation estimation integrating uncertainty and risk (probabilistic QPE) to improve the communication of severe weather and flood hazard predictability. He published his research findings in top academic journals in the fields of atmospheric sciences, remote sensing, and hydrology (more than 110 publications and three book chapters) and gave 40 invited talks worldwide. He has supervised more than 30 M.S. and Ph.D. students and post-doctoral researchers at OU, George Mason University, UC Irvine, University of Graz, Université Paris-Saclay, and Meteo France, several of whom won prizes. His research interest includes next-generation precipitation products from theoretical developments to societally relevant applications. He is an Associate Editor of the *Journal of Hydrometeorology* and *Journal of Hydrology*, the Chair of the 14th International Precipitation Conference Organizing Committee, and a member of NASA's Precipitation Measurement Missions Science Team and the Atmosphere Observing System Mission Team. He is the former Chair of AGU's Precipitation Technical Committee and NASA's Global Hydrology and Resource Center's (GHRC) User Working Group.

Hjalti H. Sigmarsson (Senior Member, IEEE) received the B.Sc. degree in electrical and computer engineering from the University of Iceland, Reykjavik, Iceland, in 2003, and the M.Sc. and Ph.D. degrees in electrical and computer engineering from Purdue University, West Lafayette, IN, USA, in 2005 and 2010, respectively.

He is currently with the School of Electrical and Computer Engineering and the Advanced Radar Research Center (ARRC), The University of Oklahoma (OU), Norman, OK, USA, where he is an Associate Professor. His current research is focused on reconfigurable RF and microwave hardware for agile communications, measurement, and radar systems. Furthermore, his research interests include spectral management schemes for cognitive radio architectures, advanced packaging utilizing heterogeneous integration techniques, and additive manufacturing of electromagnetic components.

Dr. Sigmarsson is a member of the MTT-S Technical Committee on Filters (TC-5). He was a recipient of the Best Paper Award from the IMAPS 2008 41st International Symposium on Microelectronics. In 2015, he was awarded the Air Force Office of Scientific Research (AFOSR) Young Investigator Program (YIP) to support his research on reconfigurable high-frequency components using phase-change materials. He was named a recipient of the Gerald Tuma Presidential Professorship in 2018 for meeting the highest standards of excellence in scholarship and teaching. For his outstanding support of graduate education, he was awarded the 2021 OU Graduate College Graddy Award. He is an Associate Editor of IEEE TRANSACTIONS ON MICROWAVE THEORY AND TECHNIQUES (TMTT) and the IEEE MICROWAVE AND WIRELESS TECHNOLOGY LETTER (MWTL) and the Editor-in-Chief of the *IEEE Microwave Theory and Technology Society (MTT-S) Electronic Newsletter*. In 2019, he was the General Chair of the IEEE Wireless and Microwave Technology Conference (WAMICON) and serves for the WAMICON Executive Committee. In the last decade, he has been involved in multiple conference technical program committees, such as the International Microwave Symposium (IMS), the European Microwave Conference (EuMC), the IEEE Radio Wireless Week (RWW), and WAMICON.

Tian-You Yu (Member, IEEE) received the Ph.D. degree in electrical engineering from the University of Nebraska–Lincoln, Lincoln, Nebraska, in 2000. He was with the National Center for Atmospheric Research (NCAR) as a Post-Doctoral Fellow for two years before he joined The University of Oklahoma (OU), Norman, OK, USA, in 2002. This experience has provided him with a unique cross-disciplinary background in atmospheric research using various sensors. His expertise includes the development and design of novel and sophisticated radar techniques with the goals of improving radar measurement, enhancing the warning of severe and hazardous weather, and advancing the fundamental knowledge of meteorological phenomena. Moreover, he has developed several adaptive scanning strategies and signal processing techniques leveraged on the state-of-the-art polarimetric phased array radar. In parallel with his technical strength, he has a passion for delivering high-quality education. He has developed and taught several undergraduate and graduate courses in the field of radar technology and science at OU. He is the Presidential Professor with the School of Electrical and Computer Engineering and an Adjunct Professor with the School of Meteorology, OU. He is also the Director of Operations at the Advanced Radar Research Center (ARRC), OU, which is an interdisciplinary research center.

Dušan Zrnić (Life Fellow, IEEE) received the bachelor's degree from the University of Belgrade, Belgrade, Serbia, in 1965, and the M.S. and Ph.D. degrees from the University of Illinois at Urbana–Champaign, Champaign, IL, USA, in 1966 and 1969, respectively. He is currently a Senior Scientist with the National Severe Storms Laboratory, Norman, OK, USA, and an Affiliate Professor of meteorology and electrical engineering at The University of Oklahoma, Norman. He has developed several scientific and engineering aspects of polarimetric weather radar technology leading to implementation on the WSR-88Ds. He was inducted into the U.S. National Academy of Engineering in 2006 for the development of potent radar methods that have greatly enhanced operational weather detection and warning and advanced meteorological research. He is currently a fellow of AMS. He was a recipient of the AMS Remote Sensing Prize in 2008 for pioneering and substantial contributions to the improvements of meteorological radars for both research and operational applications. He was the Chief Editor of the *Journal of Atmospheric and Oceanic Technology*.

Redmond Kelley received the B.S. and M.S. degrees (Hons.) in electrical engineering from The University of Oklahoma (OU) in 2007 and 2009, respectively. He has been a full-time Staff Engineer with the Advanced Radar Research Center (ARRC), OU, since 2009. He began his research in IF-sampling digital radar receiver technology as a Graduate Research Assistant and has since broadened his focus to radar hardware systems development. He supports most of the ARRC's hardware research projects and specializes in system-level design/integration, analog/digital circuit design, and multi-layer printed circuit board layout/fabrication/assembly. His current research interests include the design, manufacturing, and integration of cost-effective analog/digital/hybrid phased array radar technologies.

John Meier received the M.S. degree in electrical engineering from The University of Oklahoma (OU), Norman, OK, USA, in 2009. He joined the Advanced Radar Research Center, OU, in 2009. As the Lead Radar Engineer, he grows with a team capable of designing, building, and testing scalable digital-phased-array radar systems to achieve unparalleled levels of performance. He specializes in digital transceiver design, reprogrammable embedded processing, and high-bandwidth and low-latency distributed communication methods. His research interests include digital signal processing, hardware-constrained software control architectures, and phased-array radar.

Matthew Herndon (Member, IEEE) received the B.S. degree (Hons.) (magna cum laude) in computer engineering and the M.S. degree in electrical and computer engineering from The University of Oklahoma, Norman, OK, USA, in 2017 and 2022, respectively.

In 2017, he joined the Advanced Radar Research Center (ARRC), The University of Oklahoma, where he has since worked as a full-time Staff Engineer. From 2018 to 2020, he was the Software Lead for the Cylindrical Polarimetric Phased Array Radar (CPPAR) Project, during which he developed the system's control software and a novel bistatic calibration technique. He specializes in software system design/integration, data visualization, and phased array calibration. His research interests include digital signal processing, FPGA/software system design, and phased-array radar. He received the ARRC Journal Paper Award in 2021.